



Master Thesis

Mathematics

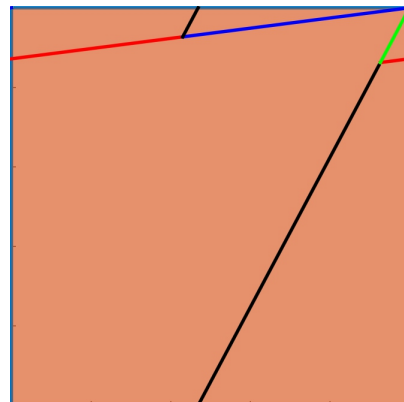
Research Group Dynamical Systems and Geometry

Neurosciences

Department of Theoretical Neurophysics

Feature integration with critical dynamics

numerical studies and mathematical analysis



Author:

Maik Schünemann

E-Mail:

mschuene@uni-bremen.de

Matr.-No.:

2926336

Address:

Kirchbachstr. 201a
28211 Bremen

Thesis advisor Mathematics: Prof. Dr. Marc Keßeböhmer

Thesis advisor Neurosciences: Dr. Udo Ernst

Submission date:

December 22, 2017

The following declarations are to be included in every exemplar of the Bachelor's and Master's Thesis

Name:

Enrolment number:

Declaration of copyright

Hereby I declare that my Master's Thesis was written without external support and that I did not use any other sources and auxiliary means than those quoted. All statements which are literally or analogously taken from other publications have been identified as quotations.

Date:

Signature

Declaration with regard to publishing theses

Two years after the final degree, the thesis will be submitted to the University of Bremen archive and stored there permanently.

Storage includes:

- 1) Master's Theses with a local or regional reference, as well as 10 % of all theses from every subject and year
- 2) Bachelor's Theses: The first and last Bachelor degrees from every subject and year

I agree that for research purposes third parties can look into my thesis stored in the University archive.

I agree that for research purposes third parties can look into my thesis stored in the University archive after a period of 30 years (in line with §7 para. 2 BremArchivG).

I do not agree that for research purposes third parties can look into my thesis stored in the University archive.

Date:

Signature

Contents

1	Introduction	2
2	Feature integration with critical subnetworks	5
2.1	The generalized EHE model	5
2.1.1	Avalanche size distributions in the homogeneous EHE Model	7
2.1.2	Finite size scaling	9
2.2	Embedding critical subnetworks	10
2.2.1	Embedding critical subnetworks without inhibition	11
2.2.2	Embedding critical subnetworks with inhibition	14
2.2.3	Capacity of the embedding algorithm	14
2.3	Separability of network dynamics for figure and background activation	19
2.3.1	2-AFC task description	19
2.3.2	Separability of avalanche size distributions	22
2.3.3	Performance of coincidence detector	27
3	Generalized EHE model	35
3.1	The generalized EHE-Model as a skew-product	36
3.2	Non-inhabited region of phase space	39
3.2.1	Decomposition of the Phase space by disjoint hyperrectangles	40
3.2.2	Self similarity of the non-inhabited volume	43
3.2.3	Recursive Decomposition of the non-inhabited region	43
3.2.4	Volume of the non-inhabited region	45
3.3	Identification of regions leading to avalanches	49
3.4	T acts bijectively on D	50
3.4.1	Invariant measure	53
3.5	The EHE Model as random walk on the N-Torus	53
3.6	Topological transitivity and ergodicity of the homogeneous EHE-Model	57
3.7	Probability Space for the avalanche patterns	61
3.8	Avalanche size distribution for the homogeneous network	61
4	Summary and outlook	64
	References	66

1 Introduction

The brain constantly receives informations about its environment from the sense organs. Perception requires that this sensory informations are integrated by the brain into a representation of the world [Schacter et al., 2011]. According to Gestalt psychology, perception is governed in the visual system by Gestalt laws stating that localized stimuli are grouped together by principles such as proximity, similarity, common fate and good continuation [Wertheimer, 1923, Wagemans et al., 2012].

Particular examples of perceptual organization are (visual) grouping and figure-background organization. Grouping integrates the features of the visual scene into wholes (*Gestalten*), and figure-background organization assigns a particular interpretation to them [Wagemans et al., 2012, Section 3].

These processes are highly complex and require sophisticated computational capabilities from the underlying neurophysiological mechanisms and a high robustness to background noise.

Theoretical considerations show that in complex dynamical systems, computational power is maximized near a phase transition between chaos and order which is called the critical state. This was first demonstrated for Boolean networks and cellular automata [Packard, 1988, Langton, 1990, Kauffman and Johnsen, 1991, Kauffman, 1993] and more recently for neural network models (see, for example, Bertschinger and Natschläger [2004], Legenstein and Maass [2007]).

An intuition for this finding is given by the following considerations [Shew and Plenz, 2013]. The dynamics of a subcritical (network) system are very unstructured and correlations between nodes decay exponentially thus information can not propagate far in the network. In a supercritical system however, initial activations quickly spread and engage the whole system, leading to 'epileptic' oscillatory states regardless of the initial conditions. The phase transition between these states where initial activation neither blows up nor dies down is termed the critical state. At such a phase transition, the system produces population events (for example avalanches in sandpile models or avalanches of spike propagation in neural network models) which are distributed according to a power law [Bak et al., 1987, Eurich et al., 2002, Levina et al., 2007b, Buice and Cowan, 2009].

Criticality in neural system is not only hypothesized in abstract neuron models but is observed in biological neural systems. Beggs and Plenz [2003] measured power law avalanche statistics with slope $-3/2$ in organotypic cultures from coronal slices

1 Introduction

of rat somatosensory cortex and acute slices using an 8×8 electrode array. After application of the GABA_A-receptor antagonist picrotoxin (weakening inhibition in the slice) epileptic discharges occurred indicative of a supercritical state. After 24hr recovery the avalanche size distribution returned to a power law of the same slope. This indicates that the neural system showed a form self organization towards this critical state. Since then evidence for criticality has been found in *vitro* and in *vivo* [Petermann et al., 2009, Ribeiro et al., 2010] although some studies found evidence against criticality [Bedard et al., 2006, Touboul and Destexhe, 2010] or report marginal subcriticality [Priesemann et al., 2014, Tomen et al., 2014]. A simple conjecture would be that the brain is not always in a critical state but uses criticality only for certain tasks. Indeed, Hahn et al. [2017] provide evidence that different vigilance states are associated with different signs of criticality and they link critical states to synchronized cortical states.

However, aside from maximizing measures of computational power like information entropy and dynamical range as described above, concrete proposals for potential benefits of criticality for a typical computaitonal task the brain has to solve are lacking.

In this thesis we propose a link between feature integration and criticality:

In particular we show that it is possible to embed subnetworks representing combinations of features belonging to a particular 'Gestalt' or 'figure' into a larger network of Eurich-Herrmann-Ernst neurons [Eurich et al., 2002]. This embedded subnetworks representing a perceptual figure display critical dynamics upon activation while subnetworks consisting of randomly chosen units not belonging to a particular figure (or the system as a whole) stay subcritical. We show that with this embedding algorithm we achieve a high capacity to embed a large number of figures with the desirable properties that neurons can simultaneously belong to several figures before the network becomes supercritical. In addition to well separated avalanche size statistics for these two modes of figure/target vs background activation fast classification is possible using a coincidence detector. We show with parametric studies that the findings are valid over a wide region of parameter space and robust to background noise and changes in the parameters of the embedding algorithm.

The Eurich-Herrmann-Ernst (in the following abbreviated by EHE) model is of special interest since the coupling strength leading to critical power law avalanche size distributions are analytically derived in Eurich et al. [2002] and extensions of this model have been successfully used as models for criticality in neural networks [Levina, 2008, Levina et al., 2007b,a].

In this thesis we extend the mathematical understanding of the EHE model. In particular we validate the derivations of the avalanche statistics in Eurich et al. [2002] by proving ergodicity based on the theory developed in [Levina, 2008, Chapter 7].

In addition we take a first step towards a comprehensive mathematical analysis of criticality in subnetworks by extending the mathematical analysis of the EHE model allowing for a general non-negative coupling matrix. We show that the qualitative

1 Introduction

properties of the EHE model dynamics generalize to this case and we extend the derivation of avalanche probabilities given in Eurich et al. [2002] to this more general case.

This thesis consists of two main parts.

In chapter 2 we provide evidence with simulation studies, that figure subnetworks, which display critical activation provide potential computational benefits for feature integration in the brain. Starting from a review of the EHE model used in this study we motivate and analyze the capacity of an algorithm constructing networks with embedded (critical) figure networks. We test the separability of avalanche size distributions between figure and background activation schemes as well as the separability using a coincidence detector in a simulated 2-alternative forced choice finding good performance over a wide region in parameter space which are qualitatively robust against changes in the embedding parameter and higher levels of background noise.

In Chapter 3 we generalize the mathematical formulation of the EHE model as a skew-product dynamical system [Levina, 2008, Chapter 7] allowing for a general nonnegative weight matrix. We are able to completely characterize the behavior of the dynamical system and show that the main qualitative properties of the homogeneous ehe system generalize to this more general setting. In addition we show that the EHE model can be understood as a skewed random walk on the torus and proof the ergodicity for the homogeneous case.

2 Feature integration with critical subnetworks

In this chapter we describe in detail the simulation studies used to evaluate whether embedded figure networks which display critical activation offer good computational abilities for feature integration.

After reviewing the dynamical regimes of the generalized EHE model and the avalanche size distributions resulting from a the homogenous system [Eurich et al., 2002] in section 2.1 we introduce the problem of constructing a weight matrix with embedded critical subnetworks in section 2.2 and analyze the transition to supercriticality of the model in dependence of number and size of embedded feature subnetworks.

In section 2.3 we show that the models with embedded subnetworks exhibit well separated dynamics depending on whether a full feature subnetwork is activated (figure activation) or a randomly chosen network (distractor activation). We start by introducing the simplified network model used in this study, which is a generalization of the EHE-model (Eurich et al. [2002]).

We say a network of EHE-model units is in the critical state, if the avalanche size distribution is close to a power law. In the critical state, (avalanche) events occur on all possible spatial and temporal scales, leading to the observation of power laws where large events are much more probable than in exponential distributions.

2.1 The generalized EHE model

In this thesis we will analyse and derive the probability distribution for the spiking behavior of a generalization of the EHE model proposed in Eurich et al. [2002]. The dynamics of the system is determined by

$$\tilde{u}_i(t+1) = u_i(t) + I_i^{\text{ext}}(t) + I_i^{\text{int}}(t) \quad (2.1)$$

$$u_i(t+1) = \begin{cases} \tilde{u}_i(t+1) & \text{if } \tilde{u}_i(t+1) < 1 \\ \tilde{u}_i(t+1) - 1 & \text{otherwise.} \end{cases} \quad (2.2)$$

We call u_i the activation value of unit $i = 1 \dots N$, with starting value in $[0, 1]$ for all

2 Feature integration with critical subnetworks

units. Throughout this thesis, N represents the number of neurons in the network (the system size).

If a unit crosses the threshold i.e $\tilde{u}_i > 1$, internal activation I_j^{int} is given to all units $j = 1 \dots N$. When using this system as a model for neural networks, the internal input corresponds to a unit giving input to other neurons by sending a spike to postsynaptic neurons.

I_i^{ext} represents external activation which is given in each time step to a randomly chosen unit, which is assumed to occur at a much slower time scale and represents, for example sensory input given to the population of neurons.

The EHE model explicitly assumes an *infinite separation of timescales*, so that external input is only given to a unit after all internal activations have died out. If the external input causes a unit to cross the threshold, an avalanche of internal inputs occurs: The activated unit resets its energy and internal activation is given to all connected units. This may push some of these units above the threshold which in turn send internal activation to the neurons connected to them.

In order to model this behavior, we introduce the vector $A(t)$ which indicates which units are above the threshold.

$$A_i(t) = \delta[\tilde{u}_i(t) > 1],$$

where $\delta[cond]$ is 1 if the condition is true and 0 otherwise. The spreading of internal activation to the connected units is mediated by a weight matrix $W = (w_{ij})_{i,j=1,\dots,N}$ with w_{ij} representing the internal activation given to unit i when unit j crossed the threshold.

$$I^{\text{int}}(t) = WA(t-1)$$

External input is applied to the randomly chosen unit $r(t)$, where $r(t) \sim \text{UNI}(\mathcal{M}), \mathcal{M} \subseteq \mathcal{N}$ and only when no internal activation is given to the system:

$$I_i^{\text{ext}}(t) = \delta[r(t) = i \wedge |A(t)|_1 = 0] \Delta U .$$

If a unit crosses the threshold, an avalanche starts. The avalanche duration $D(t)$ for the avalanche started by external input at time $t-1$ is defined as

$$D(t) := \delta[|A(t-1)|_1 = 0] \inf_{i \in \mathbb{N}} |A(t+i)|_1 = 0 .$$

The size of the avalanche is given by the number of units crossing the threshold

$$L(t) := \delta[|A(t-1)|_1 = 0] \sum_{\tau=t}^{t+D(t)} |A(\tau)|_1 .$$

Note that due to the assumption of infinite separation of timescales t does not linearly represent time but merely steps in the simulation. All steps t with $|A(t)|_1 \neq 0$ are on

2 Feature integration with critical subnetworks

the fast timescale. The time T measured on the slow time scale of the external input is given by $t - \sum_{\tau=0}^t D(\tau)$ if $|A(t)|_1 = 0$. In the following we will use the word steps to denote a step on the slow time scale. In chapter 3 we use a different approach and model this system explicitly using the separation of timescales as a discrete time skew-product dynamical system.

This dynamical system can be seen as a simplified model of a neural network. The activation value u_i represents the membrane potential of a neuron with 0 representing the resting potential. If which is above the resting potential (0) and induces a spike when it crosses a threshold, here set to 1. The spike is send to the other connected neurons. Neurons u_i is connected to neuron u_j if $w_{ji} \neq 0$ and when u_i spikes, it sends internal input to u_j that increments its activation value by w_{ji} .

However in this model neurons are *non-leaky*, i.e. their membrane potential does not decay to zero over time when receives no other activation. Additionally, after a unit spiked the membrane potential is not reseted to the resting state but wraps around without dissipation. We also note that when allowing ($w_{ij} < 0$), no lower bound is given for the activation value of the units. In this thesis we did not check the results for robustness against weaker assumptions and a more realistic model, for example a network of integrate- and fire neurons.

2.1.1 Avalanche size distributions in the homogeneous EHE Model

The model published in Eurich et al. [2002], here called the homogeneous EHE model is recovered with the choice of $W = (\frac{\alpha}{N})_{i,j \in \{1, \dots, N\}}$. Even with a constant coupling matrix, depending on the choice of α it is capable of generating different regimes of avalanche statistics, which range from an exponential, subcritical distribution through the critical point, where the avalanche size distribution is a power law for almost the complete system size, to a supercritical and multipeaked regime. Increasing α even further, avalanches can become infinitely large. This behaviour is displayed in figure 2.1.

Eurich et al. [2002] derived the closed form expression (2.3) for the avalanche size distribution using considerations involving the equilibrium density of the phase space under the assumption of ergodicity. These arguments will be extended for general matrices in chapter 3 and the ergodicity will be shown for the homogenous case.

The analytically derived avalanche size density perfectly matches the avalanche density obtained through model simulations for the regimes where avalanche sizes cannot exceed the system size.

$$p(L, N, \alpha) = L^{L-2} \binom{N-1}{L-1} \left(\frac{\alpha}{N}\right)^{L-1} \left(1 - L \frac{\alpha}{N}\right)^{N-L-1} \frac{N(1-\alpha)}{N-(N-1)\alpha} \text{ for } 1 \leq L \leq N \quad (2.3)$$

2 Feature integration with critical subnetworks

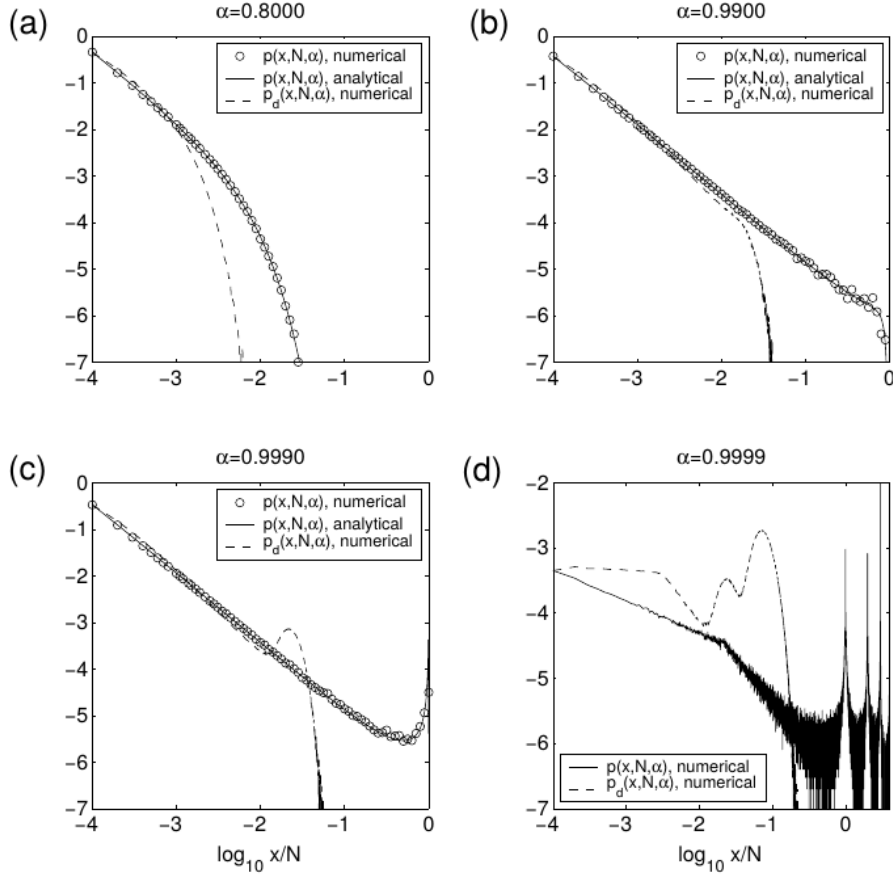


Figure 2.1: Probability distributions of avalanche sizes, $P(x, N, \alpha)$, and avalanche durations, $p_d(x, N, \alpha)$, in the subcritical (a; $\alpha = 0.8$), critical (b; $\alpha = 0.99$), supra-critical (c; $\alpha = 0.999$), and multi-peaked (d; $\alpha = 0.99997$) regime. (a-c) Solid lines and symbols denote the analytical and the numerical results for the avalanche size distributions, respectively. In (d), the solid line shows the numerically calculated avalanche size distribution. The dashed lines in (a-d) show the numerically evaluated avalanche duration distributions. In all cases, the presented curves are temporal averages over 10^7 avalanches with $N = 10000$, and $\Delta U = 0.022$. Figure and caption taken from Eurich et al. [2002].

2 Feature integration with critical subnetworks

In the limit $N \rightarrow \infty$, large avalanches are distributed according to a power law: the local exponent of the avalanche size distribution converges to $-\frac{3}{2}$ for $L \rightarrow \infty$ [Eurich et al., 2002, Eq. (9)]

$$\gamma = \lim_{L \rightarrow \infty} \lim_{\alpha \rightarrow 1} \lim_{N \rightarrow \infty} \frac{\ln \frac{p(L, N, \alpha)}{p(L+1, N, \alpha)}}{\ln \frac{L}{L+1}} = -\frac{3}{2}.$$

However, we can only perform simulations on finite size networks. For this case, the avalanche distribution is not a real power law but can be seen to have a long stretch where it fits to a log log slope of $-\frac{3}{2}$.

To find the coupling strength where the avalanche statistics most closely resembles a power law, Eurich et al. [2002] performed a numerical search for the parameter $\alpha_{\text{crit}}(N)$ minimizing the *distance* to an ideal power law $\tilde{p}(L, N) = \frac{L^{-\frac{3}{2}}}{\sum_{L=1}^N L^{-\frac{3}{2}}}$ for system sizes ranging from 10^2 to 10^7 . This *distance* between distributions was measured by the symmetric version of the Kullback-Leibler divergence $D_{KL}^{\text{sym}}(P, Q) = \sum_i (P(i) - Q(i)) (\ln(P(i)) - \ln(Q(i)))$ between $p(L, N, \alpha)$ and $\tilde{p}(L, N)$.

Using the symmetric KL-Divergence one has a divergence measure to evaluate how different two distributions are. The KL divergence is not a metric (since the triangular inequality does not hold) but it is nonnegative and zero if and only if its two arguments are the same. It is often used due to its relevance in information theoretic terms: While $D_{KL}(P, Q)$ measures the expected number of extra bits required to code samples from P using a code optimized for Q rather than the code optimized for P [Cover and Thomas, 2006, Section 2.3], $D_{KL}^{\text{sym}}(P, Q)$ represents the average number of extra bits if one distribution is coded with respect to the other one.

For finite size N the system minimizes the distance to a power law for the *critical coupling weight*

$$\alpha_{\text{crit}}(N) = \frac{1 - \frac{1}{\sqrt{N}}}{N}.$$

In order to see that the avalanche size distributions for the critical coupling scale with the exponent $-\frac{3}{2}$ and how the exponential cutoff for large avalanche sizes is related to the system size we check how whether the power law cutoff scales with the system size.

2.1.2 Finite size scaling

This section is based on [Levina, 2008, Section 3.4] using the method described in Kadanooff et al. [1989].

2 Feature integration with critical subnetworks

Assuming the finite size scaling ansatz, finite sized critical avalanches should follow a distribution given by $P_c(L, N) = N^{-\sigma} g(\frac{L}{N^\nu})$, with $\sigma, \nu > 0, g \in C(\mathbb{R}_+), g(0) \in R$. In particular σ controls the slope of the avalanche and ν how the finite size cutoff relates to the system size. For the homogeneous EHE model the correct exponents are $\sigma = \frac{3}{2}, \nu = 1$.

In order to verify this theoretical finite size scaling relation

$$P_c(L, N) = N^{-\frac{3}{2}} g\left(\frac{L}{N}\right)$$

we check if avalanche size distributions for different system sizes collapse to a single line $g(x)$ when $N^{\frac{3}{2}} P_c(L, N)$ is plotted in dependence of $x = \frac{L}{N}$.

This is done in figure 2.2 for system sizes ranging from 100 to 10000. The left panel shows avalanche distributions sampled over 10^8 avalanches from the EHE model with coupling strength $\alpha_{\text{crit}}(N)$. All these avalanche size distributions collapse to $g(\frac{L}{N})$ after rescaling. One observes a system size cutoff around $\frac{L}{N} \approx 0.85$.

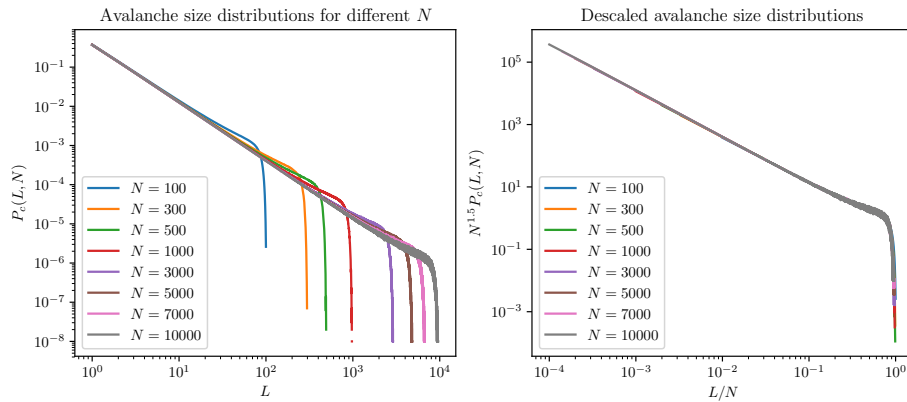


Figure 2.2: (Left) Critical avalanche distribution from 10^8 simulated avalanches. (Right) When plotting $N^{1.5} P_c(L, N)$ over $\frac{L}{N}$ all distributions collapse to a single line corresponding to the $g(\frac{L}{N})$ in the finite size scaling ansatz.

2.2 Embedding critical subnetworks

In this section we describe an approach to solve the task of embedding N_e subnetworks of N_s units each in the weight matrix W for a network of size N_u , such that these subnetworks display critical dynamics while the activity of randomly chosen units stays subcritical.

2 Feature integration with critical subnetworks

As shown in section 2.1.1 the easiest way to embed a critical subnetwork of size N_s is to take the constant weight $\alpha_{\text{crit}}(N_s)$ for all connections between elements of the subnetwork. However, when there are multiple overlapping networks, this strategy alone leads to a supercritical regime with infinite avalanches, if the coupling matrix contains no inhibitory weights.

2.2.1 Embedding critical subnetworks without inhibition

To illustrate this point, we look at a particularly simple scenario of two overlapping networks (2-olv network): We embed two subnetworks (of size $N_s = 100$ with a given overlap N_o , such that units $1, \dots, N_s$ belong to subnetwork 1 and units $N_s - N_o + 1, \dots, 2N_s - N_o$ belong to subnetwork 2. Both subnetworks are recurrently coupled with weight $\alpha_{\text{crit}}(N_s)$ and connections coupling units of different subnetworks are set to zero. See the left panel of figure 2.3 for an illustration.

We give external input to all neurons setting $M = \{1, \dots, N\}$. However, the transition to supercriticality is not dependent on the support for the external stimulation in this model. Also note that the system size scales with the amount of overlap $N = 2N_s - N_o$.

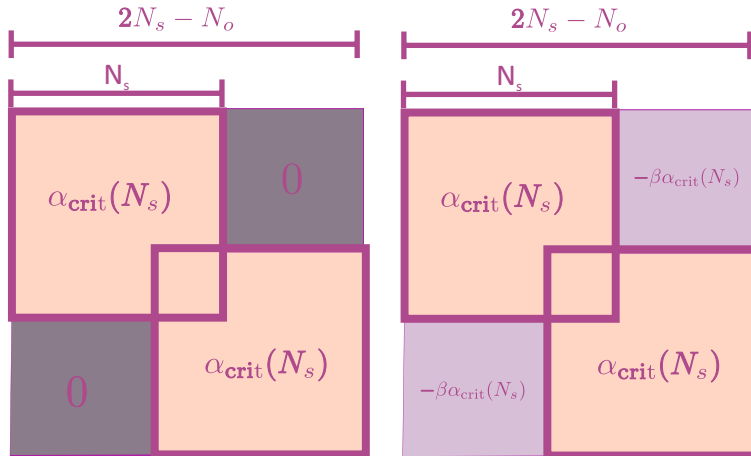


Figure 2.3: Coupling matrix for a simple 2-owl network with and without inhibition .

In this setting, there is a sharp transition to supercriticality at low values for N_o . Only for very high values of N_o , where the two subnetworks almost completely overlaps the system as a whole becomes subcritical again.

For this simple model this transition can be explained using the framework derived in chapter 3. Here we will give sufficient conditions for the avalanches to remain finite

2 Feature integration with critical subnetworks

regardless of the initial condition and the support of the external activation.

Proposition 2.2.1. *Avalanche sizes in the 2-ovl network stay finite if*

$$\begin{aligned} \left(2 - \frac{N_o}{N_s}\right) \left(1 - \frac{1}{\sqrt{N_s}}\right) &< 1 , \text{ or} \\ \left(1 + \frac{N_o}{N_s}\right) \left(1 - \frac{1}{\sqrt{N_s}}\right) &< 1 . \end{aligned}$$

Proof. We will perform a constructive proof, illustrating how the avalanche grows in size during the first few steps while calculating sufficient conditions for the avalanche to stop at each step.

First note that an infinite avalanche has to start at some point in $[0, 1]^{2N_s - N_o}$. If $u_1 \geq u_2$ componentwise for $u_1, u_2 \in [0, 1]^{2N_s - N_o}$, the size of the avalanche starting at u_1 will not be smaller than the avalanche size resulting from the starting point u_2 (this can be seen from lemma 3.1.2).

This enables us to consider without loss of generality the starting point $u^{(0)} = (1 - \epsilon)_{i=1, \dots, 2N_s - N_o}$ (with $0 < \epsilon < \min(\Delta U, \alpha_{\text{crit}}(N))$).

We now look at the fast timescale to see how the avalanche proceeds. The first few steps of the avalanche are clear: One unit receives external input which makes it fire in the first step of the avalanche. If this unit belongs to the overlap units, then in the next step all other neurons will receive input of $\frac{\alpha_c(N_s)}{N_s}$, causing them to fire at the second step. If a unit not belonging to the overlap units receives external input, it will take two additional steps until all units have fired. In the first step only the units belonging to its subnetwork receive external input and fire and in the second step the remaining units that received input from the overlap units firing in the second step. In both cases all units have fired exactly once and received input once from every connected unit thus providing a componentwise lower point the state vector

$$u_i^{(1)} \geq \begin{cases} 1 - \frac{1}{\sqrt{N_s}} - \epsilon & \text{if } i \in \text{Ovl} \\ (2 - \frac{N_o}{N_s})(1 - \frac{1}{\sqrt{N_s}}) - \epsilon & \text{otherwise ,} \end{cases}$$

where Ovl denotes the set of units in the overlap region of the two subnetworks.

A sufficient condition for the avalanche to end at this point is $(2 - \frac{N_o}{N_s})(1 - \frac{1}{\sqrt{N_s}}) < 1$.

If this condition is not fulfilled, then in the next step of the avalanche all overlap units will fire leading to the new point

$$u_i^{(2)} \geq \begin{cases} (1 + \frac{N_o}{N_s})(1 - \frac{1}{\sqrt{N_s}}) - \epsilon & \text{if } i \in \text{Ovl} \\ 2(1 - \frac{N_o}{N_s})(1 - \frac{1}{\sqrt{N_s}}) - \epsilon & \text{otherwise ,} \end{cases}$$

2 Feature integration with critical subnetworks

In order for the avalanche to stop at this point, $(1 + \frac{N_o}{N_s})(1 - \frac{1}{\sqrt{N_s}})$ has to be smaller than 1, leading to the second condition and completing the proof. \square

Figure 2.4 shows the phase space of this 2ovl network and the calculated sufficient conditions for the nonexistence of infinite avalanches.

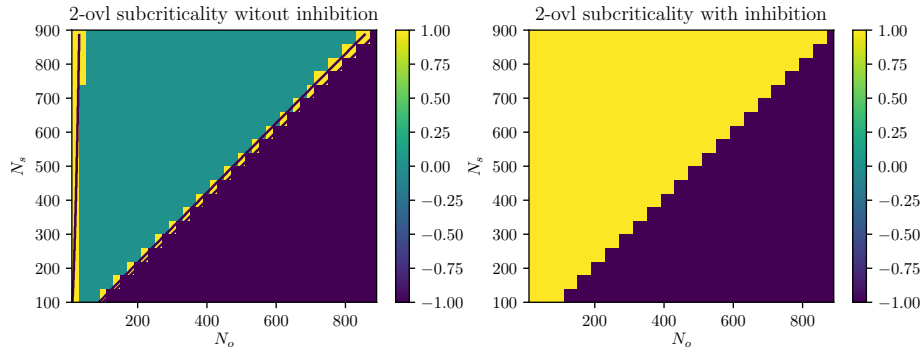


Figure 2.4: Subcriticality index for the 2-ovl network with and without inhibition.

The subcriticality index is simulated for $N_s = 100, 140, \dots, 900$ and $N_o = 10, 30, \dots, 900$). Left panel: Without inhibition, only a small fraction of the available phase space $N_o \leq N_s$ is subcritical. The contour lines indicate the analytical transition boundary according to proposition~2.2.1. Right panel: With inhibitory connections of $-\alpha_{\text{crit}}(N_s)$ between units not belonging to the overlap there is no supercritical region in the available phase space.

This leaves only a tiny portion of the phase space for a functional, not supercritical, network. The intuitive explanation for the transition to supercriticality in this model is the crosstalk excitation given to the subnetworks by the units in the overlap. These overlap units receive input from all neurons, thus they react like being in a subnetwork of size $2 * N_s - N_o$ but with coupling strength suitable for a network of size N_s .

If N_0 is not very large, the coupling strength $\alpha_{\text{crit}}(N_s)$ is far in the supercritical regime for a network of size $2 * N_s - N_o$, which allows the overlap units to fire multiple times. In order to cause the system as a whole to have infinite avalanches, the supercritical overlap units have to spread enough activation to the other units of the networks to make them fire multiple times. This happens only for sufficiently many units in the overlap.

A possibility to enlarge the functional portion of the phase space one could choose a smaller coupling parameter than α_{crit} for the subnetworks. However, this would lead to subcritical dynamics if only one network receives external input. Instead we consider the possibility of containing the excitatory crosstalk between networks by inhibitory weights between units belonging to no common subnetwork.

2 Feature integration with critical subnetworks

We now add inhibitory weights of $-\alpha_{\text{crit}}$, or more generally with weight $-\beta\alpha_{\text{crit}}$ between nodes not sharing a common subnetwork, as is illustrated in the right panel of figure 2.3. The resulting inhibition manages to completely contain the excitatory crosstalk, even for $\beta = 1$, and the whole phase space stays functional (right panel of figure 2.4).

2.2.2 Embedding critical subnetworks with inhibition

We now describe an algorithm to construct suitable weight matrices which produce critical avalanche dynamics when a subnetwork is activated but stay subcritical if a random subset of units is activated.

To embed N_e such subnetworks, one iteratively selects N_s distinct units from the set $\{1, \dots, N_u\}$ and setting the coupling strength for connections between the selected units to $\alpha_{\text{crit}}(N_s)$.

As seen in section 2.2.1, it is important to suppress the crosstalk excitation by sending inhibition between units having no common subnetwork. For simplicity we also choose a constant value for the inhibition given by $-\beta\alpha_{\text{crit}}(N_s)$.

The algorithm consists of the following steps:

- Initialize the weight matrix W of size $N_u \times N_u$ with values $-\beta\alpha_{\text{crit}}(N_s)$
- Repeat N_e times:
 - Uniformely choose N_s elements from the set $\{1, \dots, N_u\}$ without replacement and assign it to I
 - Set the submatrix formed by the rows and columns in I to $W_I = \alpha_{\text{crit}}(N_s)$.

Weight matrices created by this algorithm are shown in figure 2.5. By construction every such weight matrix is symmetric, contains only the values $\alpha_{\text{crit}}(N_s)$, $-\beta\alpha_{\text{crit}}(N_s)$ and every unit is positively coupled to either at least N_s units (including itself) or to no unit at all if it does not belong to any subnetwork.

Up to reordering of the units and removing not selected units, the case of embedding two subnetworks reduce to the 2-ovl network analyzed in section 2.2.1.

2.2.3 Capacity of the embedding algorithm

Similar to the purely excitatory 2-ovl network analyzed previously, we investigate the 'capacity' of this embedding scheme: How many subnetworks of a given size can be embedded before the system becomes supercritical?

2 Feature integration with critical subnetworks

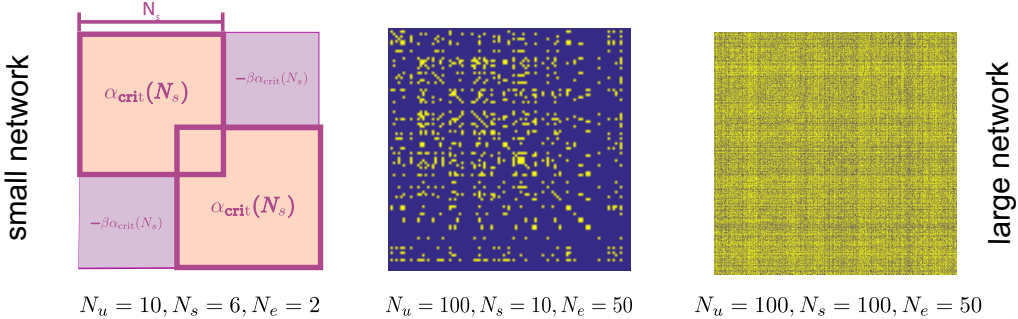


Figure 2.5: Illustration of weight matrices from small network size to larger number of units and number of subnetworks. We will perform our simulations on networks with similar parameters as the large network displayed in the right panel.

We introduce the subcriticality index I_{sub} to be the probability that avalanche sizes stay finite (regardless of the external input support) for a realization of the weight matrix sampled with parameters $N_u, N_s, N_e, \beta \backslash \beta$.

Since in this case the system size always stays constant (N_u) and the weight matrix contains more excitatory and less inhibitory connections when for fixed N_s the number of subnetworks N_e is increased, we have for each N_s at most one transition point into the supercritical regime. See the first three subplots of figure 2.7 for the subcritical index plotted over the phase space spanned by N_e, N_s for three values of $\beta = 1, 2, 3$ representing low, medium and high levels of inhibition.

This shows that we have found a way to embed subnetworks into a larger inhibitory network that has a very high capacity to form a functional network with finite avalanche sizes. We use the number of subnetworks one unit belongs to on average as a measure for the capacity. Figure 2.6 shows the maximal capacity (capacity evaluated at the median of the transition boundary) in dependence of N_s for $\beta = 1, 2, 3$.

Numerically, the transition boundary on the phase space was calculated as follows: I_{sub} is approximated by the fraction of sampled weight matrices producing finite avalanches for 20 realisations of weight matrices generated by the embedding algorithm. We use the following procedure to (approximately) check whether the network is able to generate infinite avalanches:

Like in the purely excitatory case considered above, we set the initial values close to 1 for the simulations ($u_i = 1 - \epsilon$ for all $i \leq N_u$). We now give external input to one random unit and observe if the resulting avalanche stops after 100 fast timescale steps. The validity of the resulting transition boundary calculated with this simplifying assumption was checked by comparing it to the transition boundary for the results of section 2.3.3 (see figures 2.15, 2.10). In these simulations not just one but 10000

2 Feature integration with critical subnetworks

avalanches were simulated using uniformly chosen random initial values. The criterion to check if an avalanche doesn't stop was to wait 10000 fast timescale steps and for each parameter set N_s, N_e simulations were performed with different realizations and supports for the external activation.

In addition we used the property that there can be only one transition to supercriticality for a given N_s with increasing N_e to perform an efficient numerical search for the transition boundary in the parameter space: Given a pair of N_s, N_e first search in the direction of decreasing N_e until the subcriticality index is 1 and then search in the direction of increasing N_e until the subcriticality index is 0. Now proceed to neighboring N_s with the median point of the observed transition region as new starting value of N_e .

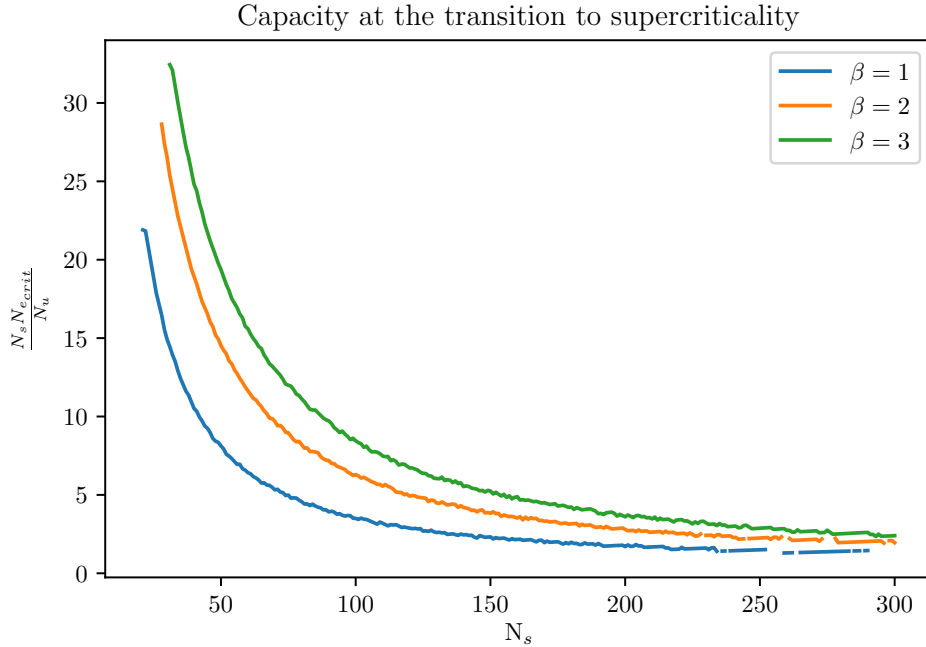


Figure 2.6: Capacity (average number of subnetworks that a single unit belongs to) at the transition to supercriticality $N_{e_{crit}}(N_s)$ in dependence of N_s for different levels of inhibition $\beta = 1, 2, 3$.

We now take a closer look at the transition boundary to the supercritical regime. Similar to the behavior of the purely excitatory network when started at in the state $u = (1 - \epsilon)_{0 < i \leq N_u}$ the unit starting the avalanche pushes all the units that share a common subnetwork while inhibiting the rest. In the second fast timescale step of the avalanche all these connected units fire and give excitatory input to all units sharing a common subnetwork with them and sending inhibition to the rest. This *oscillatory* spiking activity subsides after the first few fast timescale steps in the subcritical regime

2 Feature integration with critical subnetworks

while it sustains itself in the supercritical regime. Since the number of units that share an excitatory connection with a given unit controls the amount of excitation given to the network the percentage of excitatory vs inhibitory connections of a units a prime candidate for a control parameter describing this phase boundary.

We can analytically compute the probability that two units do not share at least one common subnetwork and therefore inhibit each other: Let u_i, u_j with $i, j \leq N_u$ be two arbitrary units in a realization of the embedding scheme for parameters N_u, N_s, N_e . We want to calculate the probability that u_1 and u_2 are disconnected, i.e not belonging to a common subnetwork. If $i = j$ this probability is trivially zero. If $i \neq j$ we use the fact that all subnetworks are drawn independently from each other and fix one subnetwork s_1 containing u_i . The $N_s - 1$ other units belonging to this subnetwork are independently drawn without replacement (hypergeometric distribution) from the remaining $N_u - 1$ units. The probability that none of these units is u_i is given by $\frac{N_u - 2}{N_s - 1} / \binom{N_u - 1}{N_s - 1} = 1 - \frac{N_s - 1}{N_u - 1}$. The expected number of subnetworks a unit is connected to is given by $\frac{N_e N_s}{N_u}$. Thus the probability for two units to be not excitatorily connected is

$$P[\text{two units are disconnected}] = \frac{N_u - 1}{N_u} \left(1 - \frac{N_s - 1}{N_u - 1}\right)^{\frac{N_s N_e}{N_u}}. \quad (2.4)$$

The bottom right panel of figure 2.7 shows this probability in dependence on N_s, N_e including contour lines of levels 0.4, 0.5, 0.68 which most closely follow the transition boundary to supercriticality for $\beta = 3, 2, 1$.

In this section we have shown that it is possible to embed a high number of subnetworks in a bigger network while the system as a whole remains in a functional state producing finite avalanches without runaway activity. We made no special assumptions about the structure of subnetworks and tested the embedding algorithm with independently drawn subnetworks that were chosen by uniformly selecting distinct units.

The transition region to the supercritical region was numerically calculated for large parts of the phase space and shown to be closely connected to the ratio of excitatory and inhibitory connections of a unit on average.

Up to now functionality was equated with producing finite avalanche sizes, but in order to use these networks for feature integration we have to show that the dynamics in activated feature-subnetworks is different than the dynamics in activated subnetworks chosen randomly.

2 Feature integration with critical subnetworks

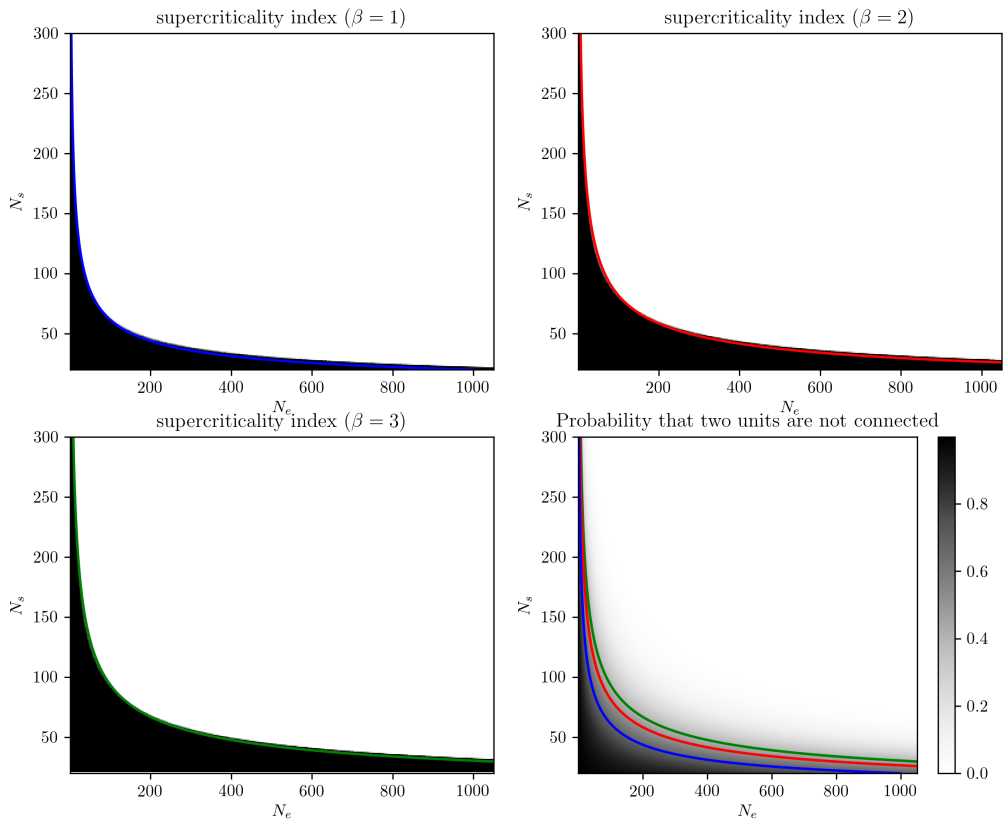


Figure 2.7: Phase space of the probabilistic embedding algorithm with inhibition in dependence on N_s, N_e for $N_u = 1000, \beta = 1, 2, 3$. The top row and the lower left panel show numerically evaluated subcriticality indices indicating the probability that avalanche sizes stay finite. This region becomes larger for increasing β . The lower right panel shows a heat plot of the probability that two units don't share a common subnetwork. The contour lines (blue=0.68, red=0.5, green=0.4) indicate levels closely describing the phase transition boundary observed for $\beta = 3, 2, 1$.

2.3 Separability of network dynamics for figure and background activation

After we have successfully developed an algorithm which can embed a high number of subnetworks we are now going to test whether these embedded figure subnetwork show clearly separate dynamics from randomly chosen activated networks.

We test this by simulating a 2-alternate forced choice task, which is a standard paradigm in behavioral contour integration experiments. Contour integration is a special case of perceptual grouping in which oriented line elements are perceived as a contour when they are aligned according to Gestalt laws like the law of good continuation. In particular this process is thought to occur in the early stages of visual perception in the brain in the striate cortex, and there is evidence for an association field [VanRullen et al., 2001, Yen and Finkel, 1998, Li and Gilbert, 2002, Field et al., 1993]. Similar to the coupling scheme considered here, the association field puts excitatory connections between stimuli (or neurons receptive to stimuli) that are well aligned while proposing inhibitory connections between misaligned stimuli. In this respect it shares some similarities with the embedding matrices considered in this thesis and can serve as an illustration for the general principle of feature integration. See figure 2.8 for an illustration of our proposed avalanche dynamics for the example of contour integration.

In this section, we will introduce the 2-AFC task and evaluate two key properties our networks should have:

- Well separated avalanche statistics, with activated figure networks displaying critical behavior
- Well separated temporal dynamics which can be used to differentiate in short time between the dynamics of an activated figure network and a randomly chosen one.

2.3.1 2-AFC task description

To evaluate the computational capabilities of the proposed approach we model a 2-alternative forced choice (2-AFC) task which is a standard paradigm in behavioral experiments.

In a 2-AFC experiment, the proband is presented two stimuli, a *target* stimulus containing a figure and a *distractor* stimulus containing only randomly oriented background elements. The task of the proband is to detect the target stimulus. The contour integration 2-AFC task is made harder for the participant if the contrasts of the stimuli are varied. Human participants nevertheless can easily distinguish the figure in the target stimulus with less background contrast from the random elements presented in the distractor stimulus.

2 Feature integration with critical subnetworks

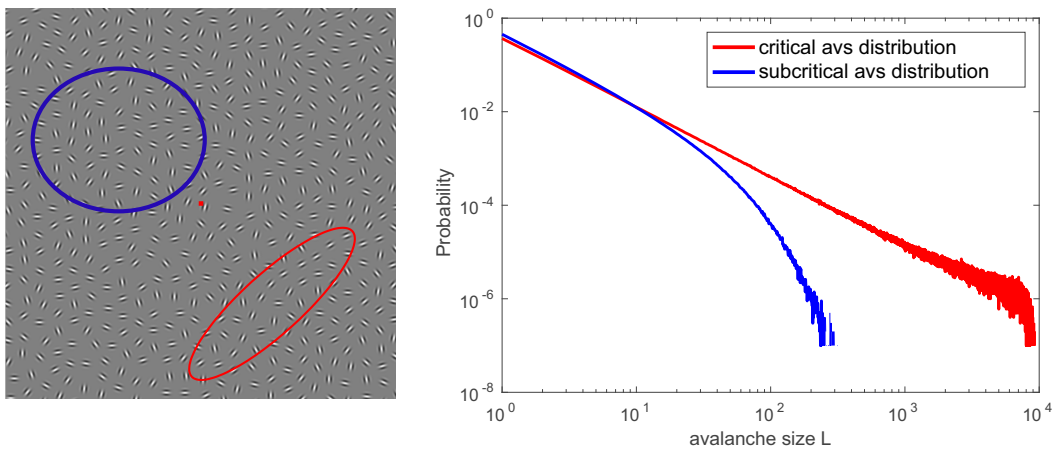


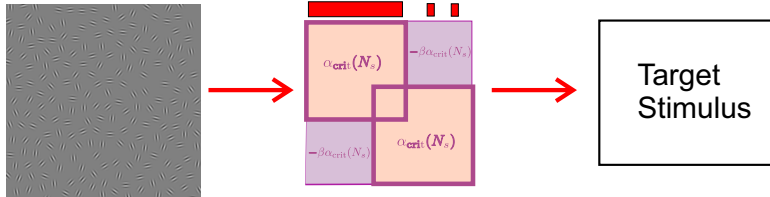
Figure 2.8: Proposal for critical avalanche statistics in subnetworks for contour integration. The left panel shows a stimulus used in psychophysical contour integration experiments. The task of the proband is to identify whether there is a contour shown at some position of the stimulus or whether it only consists of randomly aligned bar elements. The blue region marks a region of only randomly oriented background elements while there is a contour of co-aligned orientation elements in the red region. Sampling avalanches from the blue region will result in a subcritical avalanche size distribution while the activity of the elements belonging to the aligned contour becomes critical (right panel) .

2 Feature integration with critical subnetworks

We simulate the 2-AFC task in the following way: For given parameter values N_s, N_e, K, β we construct a weight matrix with N_e subnetworks of size N_s using the embedding algorithm with inhibition level β . We distinguish between the target and distractor case by activating (giving external input to) different sets of units. For the target stimulus, we activate one whole feature subnetwork and K additional randomly selected units. The same number $N_s + K$ units are given external input in the distractor stimulus, but here these units are randomly chosen. The target and distractor stimuli consists of the spiking activity recorded from the weight matrix with this different activation schemes. For each parameter set N_s, N_e, K, β 10000 avalanches were recorded for 10 different realization of the embedding matrix and 10 different choices of activated subnetwork and random background elements.

The correspondence between the contour integration task and the performed simulations are illustrated in figure 2.9.

-Target/(figure embedded): randomly chosen figure subnetwork + K random background units



-Distractor/(no figure,background elements only): $N_s + K$ randomly chosen background units

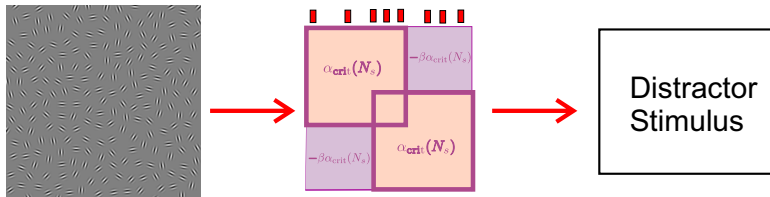


Figure 2.9: Illustration of stimuli used for the 2-AFC-Task . Left: Examples of visual stimuli used in contour integration 2-AFC tasks. Middle: Support for the external activation given to the EHE model is visualized by red bars on top of the elements receiving external input. Right: Spike trains arising from this model constitute the Target and Distractor stimuli. The visual stimulus that the proband gets presented are represented by spike trains arising from an EHE model with N_e embedded subnetworks of size N_s . When this visual stimulus contains a contour, i.e. multiple patches oriented similarly and located colinearly/cocircularly, this is modeled by giving activation to a whole embedded subnetwork whereas the units receiving external input are chosen randomly for the distractor stimulus. In this example, the visual Target stimulus has a lower background contrast than the Distractor stimulus. This is incorporated into the model by scaling overall firing rates.

2 Feature integration with critical subnetworks

In order to simulate changes in the background contrast we scale the global firing rates. We show that the coincidence detector described in section 2.3.3 can distinguish between target and distractor even for the case of low background contrast in the target stimulus, where the global firing rates are equal in both stimuli.

Adjusting the global firing rates could be done in two different ways in the simulation. The first way is to adjust the strength of the external input ΔU . Since the dynamical system just performs a random walk along the positive directions of the axes, the time between two spiking events is inversely related to ΔU . However, this approach bears some difficulties. First, the qualitative behavior of the dynamical system may change for too large values of ΔU , for the generalized EHE model without inhibition the condition $\sum_{j=1}^N w_{ij} + \Delta U < 1$ is a fundamental assumption for all results stated in chapter 3. Changing the values of ΔU is also not physiologically plausible since ΔU represents input from other (sensory) neurons.

Instead we use a simpler procedure that allows to change the background contrast after the simulation, but discards some samples, by scaling not ΔU but the time T . For the target stimulus time is equal to the number of external stimulation steps, while for the background contrast adjusted distractor stimulus it is given by the number of external stimulation steps divided by the background contrast.

2.3.2 Separability of avalanche size distributions

In this section we evaluate the separability of the avalanche size statistics arising in the target vs the distractor stimuli. We find that over a large part of parameter space avalanche statistics are well separated between Target and Distractor stimuli, with the avalanche statistics in the Target being close to critical vs the subcritical avalanche distribution arising in the Target stimulus.

For the parameters $\beta = 2, K = 100$ and $40 \leq N_s \leq 70, 80 \leq N_e \leq 116$ Figure 2.10 shows the discriminability of Target and Distractor avalanche dynamics over the phase space. The figure in the top row depicts the simulated phase space and shows the transition to the supercritical phase, which coincides with the transition boundary shown in figure 2.7. Before the transition region, all 100 simulations produced 10000 avalanches each for both the target and distractor stimuli, leading to 2×10^6 avalanches. On the transition boundary some of the 100 simulations produced infinite avalanches while inside the supercritical region the networks produced no avalanche of finite size. Numerically the simulation was stopped if an avalanche continued after 10000 steps on the fast time scale.

For points being far away from the transition region, avalanche size distributions are very well separated, see bottom left panel of figure 2.10. The avalanche size distribution in the Target for this realization is close to a critical distribution, as this distribution closely coincides with a reference avalanche size distribution which was sampled from a homogeneous EHE model of size N_s using the same number of

2 Feature integration with critical subnetworks

avalanches as produced by the 2-AFC Target stimuli. When approaching the transition boundary, the subcritical avalanche size distribution in the Target stimuli becomes closer to the still critical Target avalanche size distribution, see the bottom middle panel of figure 2.10. The bottom right panel shows the avalanche size distributions for a point on the transition boundary. Here, target and distractor distribution can become very similar, before - when further increasing N_e - they become supercritical and infinite.

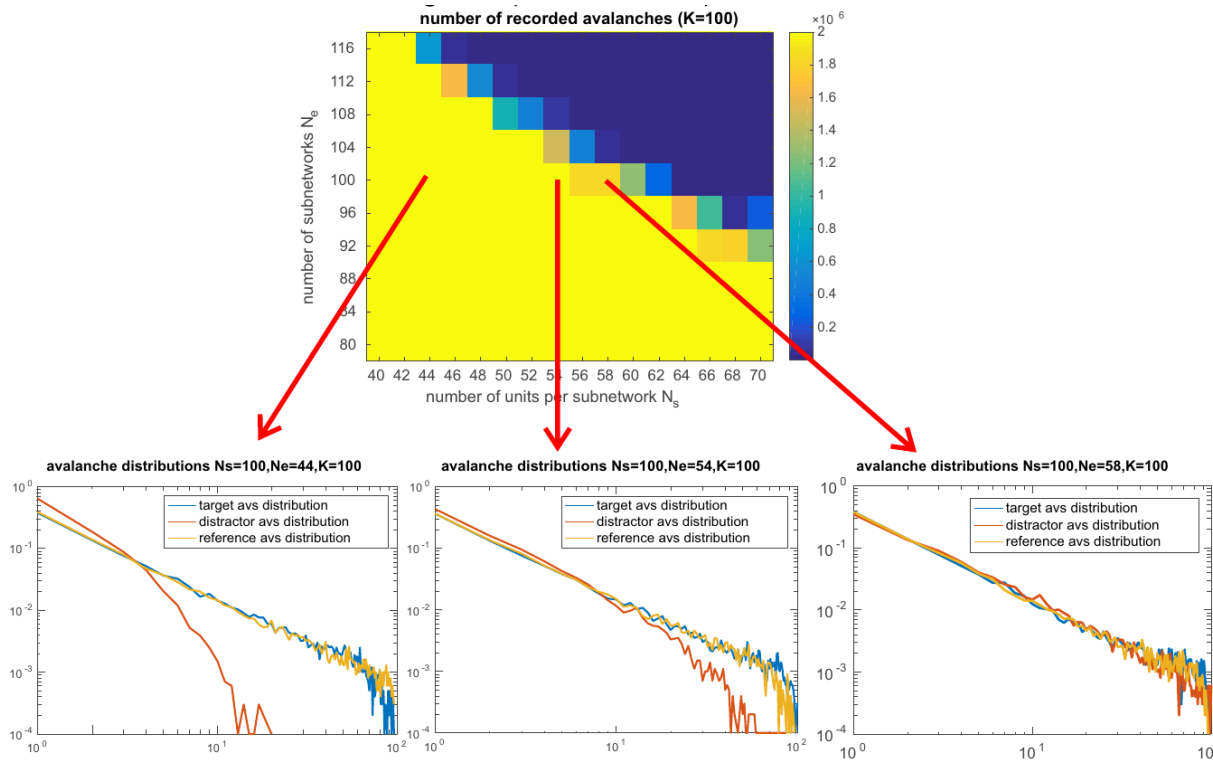


Figure 2.10: Avalanche statistics in the 2-AFC task . The top panel shows the phase space of the 2-AFC simulations. The yellow area marks the subcritical region where all realisations produced finite avalanches. The transition region to supercriticality coincides with the one observed in figure reffig:phase-space (b). The bottom row shows the observed avalanche statistics for different points in phase space indicated by the red arrows. The Target avalanche size distribution stays similar to a reference critical distribution while the Distractor distribution is subcritical, but becomes more and more critical with decreasing distance to the supercritical region.

2 Feature integration with critical subnetworks

The separability of the avalanche size distribution can be understood by inspecting spike raster plots resulting from the 2-AFC simulation, which are shown in figure 2.11. After the first avalanches, which have a chance to occur both in the figure and activated background units depending on the initial conditions and sequence of external inputs, the figure units quickly win the competition and due to the all-to-all inhibition all nonfigure units are silenced during the rest of the simulation, and the model behaves just as the critical ehe-model in the subnetwork. The activation pattern in the Distractor stimulus is unlikely to favor a particular embedded subnetwork significantly more than others and activation stays spread over more than one subnetwork.

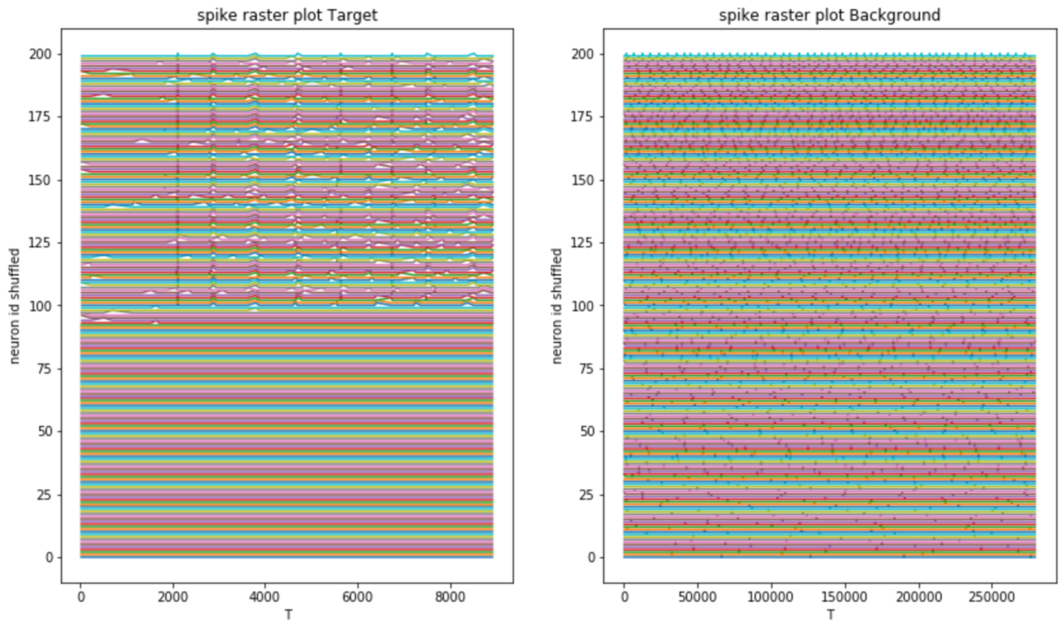


Figure 2.11: spike raster plot for 2-AFC simulation with parameters $N_s = 100, N_e = 500, K = 100, \beta = 2$ for Target (left) and Distractor (right) stimuli. (a) neurons 100-200 are figure units and 0-100 background units receiving external input ordered by their total spike count. (b) 200 most active units, sorted by their total spike count

To check whether this separability is robust with respect to the other parameters, simulations were done with higher number of random background units receiving external input $K = 200$, and also with the embedding parameter β set to one in which case the inhibitory connections are only halve as strong.

The top row of figure 2.12 shows that this qualitative behavior stays the same even for $K = 200$ while the bottom row shows the same for $\beta = 1$

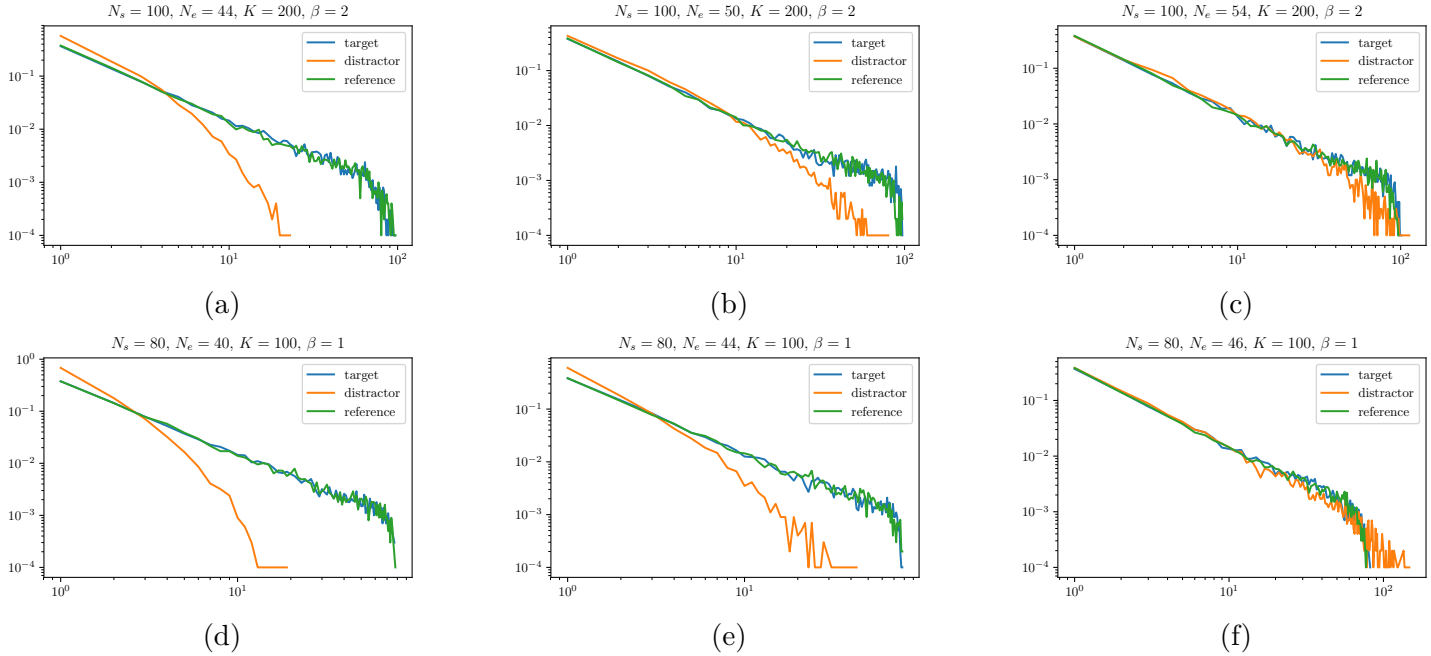


Figure 2.12: Avalanche plots for $\beta = 2, K = 200$ (top row) and $\beta = 1, K = 100$ (bottom row). TODO thicker lines etc. etc. maybe draw one smooth reference distribution instead of reference distributions sampled with the same number of avalanches

2 Feature integration with critical subnetworks

2.3.3 Performance of coincidence detector

In order to make practical use of criticality in subnetworks for feature interation, the brain has to distinguish between feature and random subnetworks in a short amount of time. In particular, it cannot wait a long time to sample sufficient avalanches until it is clear that one avalanche size distribution resembles a power law.

Here we investigate the performance of a simple coincidence detector, which can easily be realized by neural mechanisms (discussed below), to show that the different dynamics between target and distractor can be differentiated in a short time. Here we measure time T on the slow timescale of the external input.

The coincidence detector records large (synchronous) events and uses the number of observed synchronous events to distinguish between target and distractor. A possible neural realization would be a single readout neuron, for example a linear integrate and fire neuron, receiving input from afferent neurons with firing threshold and synaptic gain tuned to a level such that only multiple synchronous afferent spikes can elicit a postsynaptic spike.

The coincidence detector is parameterized by the avalanche size threshold for synchronous events s_0 and is given an allowed observation time T . It receives as input the spike trains from the target avs_1 and distractor avs_2 stimuli sampled during this time horizon T .

It outputs 1 to indicate avs_1 comes from the target and 2 for avs_2 . The coincidence detector bases its decision on the sizes of avalanches occurring at each time step. It records whether the size crosses the threshold s_0 . The number of these synchronous events for the input avalanches is compared and the time series with the higher number is given the target label. In case where in both time series the same number of synchronous events is recorded, it picks randomly.

This is formalized by the following classifier:

$$\text{coince}_{s_0}(\text{avs}_1^T, \text{avs}_2^T) = \begin{cases} 1 & \text{if } \sum_{\text{av}_1 \in \text{avs}_1^T} \delta[\text{size}(\text{av}_1)] > \sum_{\text{av}_2 \in \text{avs}_2^T} \delta[\text{size}(\text{av}_2)] \\ 2 & \text{if } \sum_{\text{av}_1 \in \text{avs}_1^T} \delta[\text{size}(\text{av}_1)] < \sum_{\text{av}_2 \in \text{avs}_2^T} \delta[\text{size}(\text{av}_2)] \\ 1 + U & \text{otherwise, } U \sim \text{Ber}(0.5) . \end{cases}$$

Denote by $\text{syn}_1^T, (\text{syn}_2^T)$ the random variables representing the number of synchronous events during T external stimulation timesteps in the target (distractor) stimulus with support $0, \dots, n_1^T (0, \dots, n_2^T)$. The accuracy of coince_{s_0} with time horizon T is then calculated by

2 Feature integration with critical subnetworks

$$\begin{aligned}
P[\text{coince}_{s_0}(\text{avs}_1^T, \text{avs}_2^T) = 1] &= P[\text{syn}_1^T > \text{syn}_2^T] + \frac{1}{2}P[\text{syn}_1^T = \text{syn}_2^T] \\
&= \sum_{i=1}^{n_1^T} P[\text{syn}_1^T = i] P[\text{syn}_2^T \leq i - 1] + \frac{1}{2}P[\text{syn}_1^T = \text{syn}_2^T] \\
&= \sum_{i=1}^{n_1^T} P[\text{syn}_1^T = i] \sum_{j=0}^{i-1} P[\text{syn}_2^T = j] + \frac{1}{2}P[\text{syn}_1^T = \text{syn}_2^T] \\
&= \sum_{i=1}^{n_1^T} P[\text{syn}_1^T = i] \sum_{j=0}^i \frac{1}{1 + \delta_j^i} P[\text{syn}_2^T = j]
\end{aligned}$$

and thus directly available given empirical histograms of $\text{syn}_1^T, \text{syn}_2^T$. When performing an Receiver-Operator Characteristic with this two distributions $\text{syn}_1^T, \text{syn}_2^T$, the accuracy of the coincidence detector is given by the area under the curve.

The coincidence detector is evaluated for each 2-AFC simulation with parameters s_0, T logarithmically scaled between 20 and 1000, and linearly scaled between (0, 20).

We are now going to present the performance results of the coincidence detector over the 2-AFC phase space starting from a close look at a specific realization $N_s = 100, N_e = 50, K = 100, T = 1000, s_0 = 30$ and we describe how the coincidence distributions $\text{syn}_1^T, \text{syn}_2^T$ arise from a population plot for this parameters.

We study the dependence of the 2-AFC accuracy on the coincidence detector parameters s_0, T for fixed 2-AFC parameters N_s, N_e, K, β and show that for fixed T there exists an optimal s_0 maximising the accuracy. Finally we look at the maximal performance and optimal threshold over the 2-AFC phase space N_s, N_e and check robustness of these results with respect to increased background activation K and lower levels of inhibition β .

Figure 2.13 shows a section of the population activity in the target and distractor stimuli with parameters $N_s = 100, N_e = 50, K = 100, \beta = 2$, adjusted background contrast of $bc = 4.56$, and with coincidence detector parameters parameters $s_0 = 30, T = 1000$.

This gives rise to the threshold distribution shown in panel (c) of figure 2.14. Figure 2.14 shows the distributions $\text{syn}_1^T, \text{syn}_2^T$ for parameters $N_s = 100, N_e = 50, K = 100, T = 1000, \Delta U = 0.022$ and different thresholds $s_0 = 1, 24, 30, 45$. The maximal accuracy of the coincidence detector is reached for parameter $s_0 = 300$ shown in panel (c).

Panel (a) shows the distributions for avalanche size $s_0 = 1$, which reduces to the number of avalanches occurring in the allowed Time horizon. Here the distributions from target and distractor are most clearly separated which is easy to understand. The average avalanche sizes in the target stimulus is much higher but the overall rates

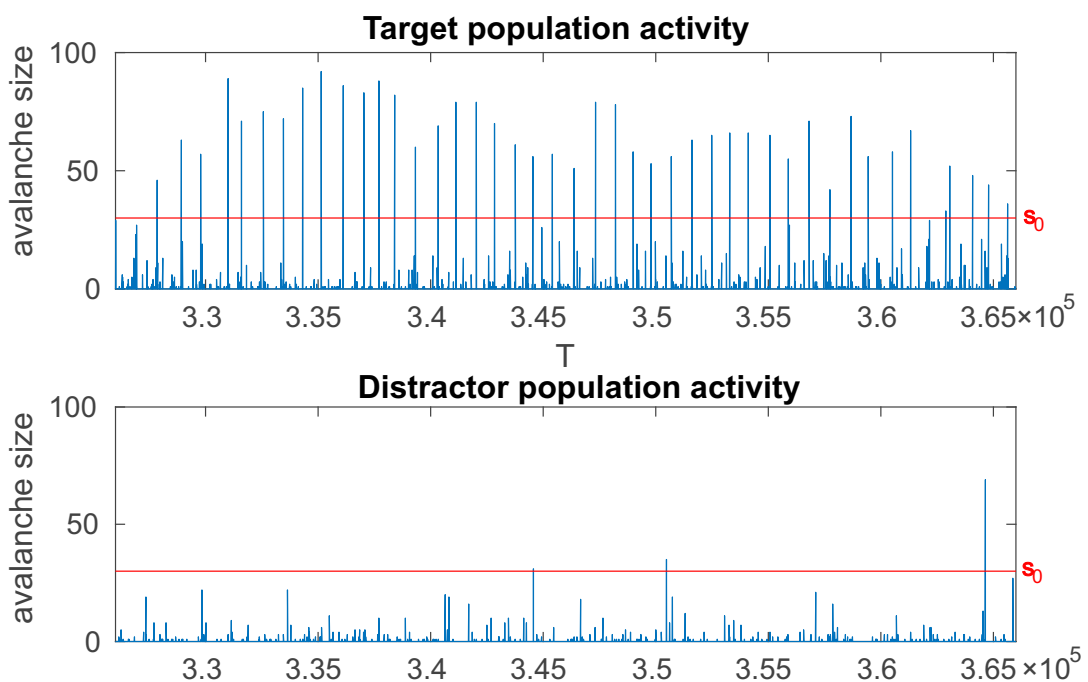


Figure 2.13: Population activity in background contrast adjusted target and distractor stimulus for parameters $N_s = 100, N_e = 50, K = 100, \beta = 2, s_0 = 30, T = 1000$.

2 Feature integration with critical subnetworks

are kept equal, which means that the number of occurring avalanches in the distractor stimulus is much bigger than the number of avalanches occurring in the avalanche input. However detecting just the number of occurring avalanches would mean having a neuron in the neurophysiological realization tuned such that every single arriving spike causes it to fire, which is physiologically implausible.

Looking through panel (b)-(d) we see that up to $s_0 = 30$, the separability of Target and Distractor distributions increases, but for larger s_0 it decreases again. The existence of an optimal threshold of intermediate size can be explained like follows:

When s_0 is too low, not just avalanche sizes resulting from the target stimulus cross the threshold but also many avalanches from the distractor stimulus, decreasing the separability of the distributions syn_1^T and syn_2^T . If on the other hand s_0 is too large, then even for the target stimulus it is very rare to have one or two avalanches with sizes bigger than s_0 during the time horizon T , which narrows the support of the distribution and reduces separability from the distractor threshold distribution, which is almost fully supported on zero.

2 Feature integration with critical subnetworks

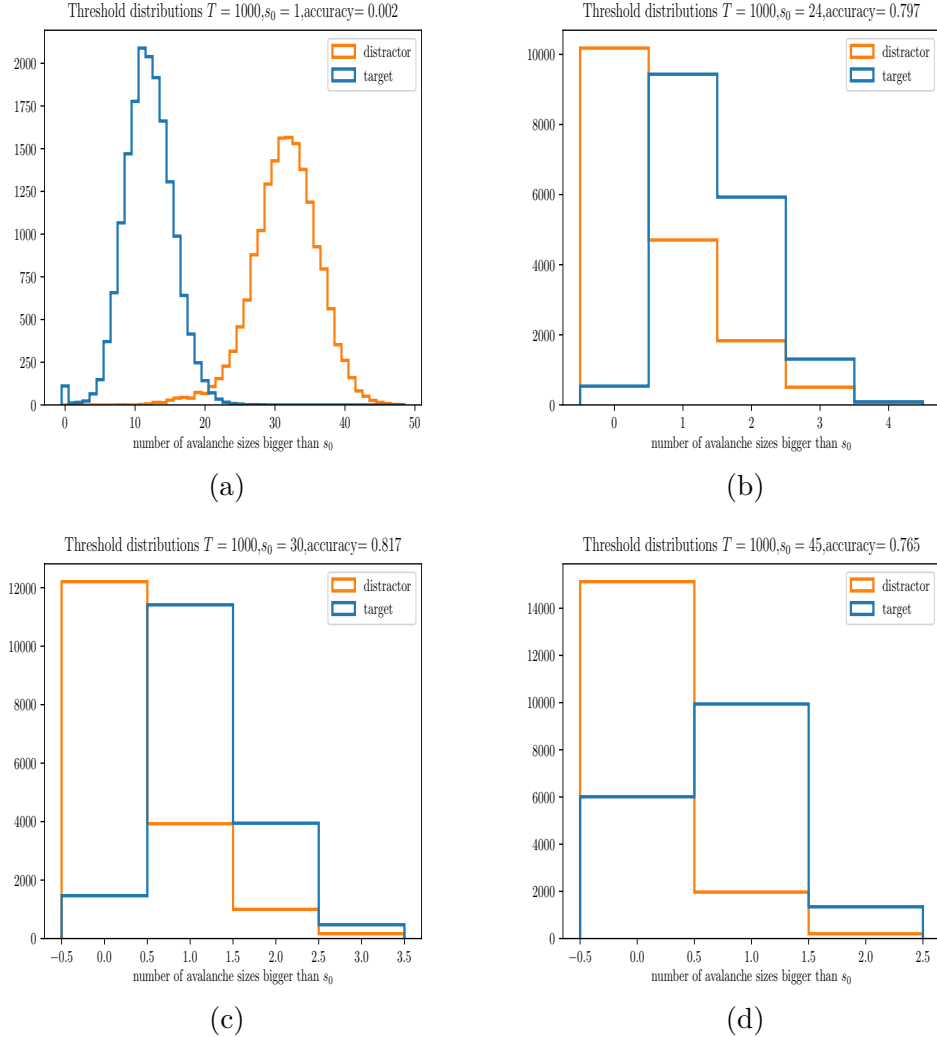


Figure 2.14: $\text{syn}_1^T, \text{syn}_2^T$ for parameters $N_s = 100, N_e = 50, K = 100, T = 1000, \Delta U = 0.022$ and different thresholds $s_0 = 1, 24, 30, 45$.

Going up a level we can draw 2-AFC accuracy heat plots over all parameters s_0, T and fixed N_s, N_e, K, β , see figure 2.15. In each heat plot the line connecting the s_0 values maximising the accuracy for fixed T is shown in red. Comparing the heatplots shown for $N_e = 42, 50, 54$ one notices a decrease in the maximal accuracy obtainable and for a large parameter range an increase of the maximal s_0 with increasing N_e .

Going even another level up we plot a heat map of the best accuracy for a specific $T = 10000$ over the 2-AFC simulation phase space shown in panel (c) of figure 2.15.

One notices that approaching the transition region to supercriticality performance decreases while on the transition region also high maximal accuracys can be obtained.

2 Feature integration with critical subnetworks

This is explained by some realizations producing zero avalanches while others are just short the supercritical regime but having very well separated avalanches.

Overall, figure 2.15 shows that the coincidence detector achieves very high accuracy in the 2-AFC task over a wide range of parameters, thus showing that detecting the activation of a critical subnetwork can easily be done with a neurophysiologically realizable coincidence detector. Note that the best accuracies increase inside the transitioning region to criticality. This is explained by the observation that in this region many realizations of the weight matrix display supercritical behavior, but for the realizations which produce finite avalanches, the dynamics between target and distractor can be easily discriminated.

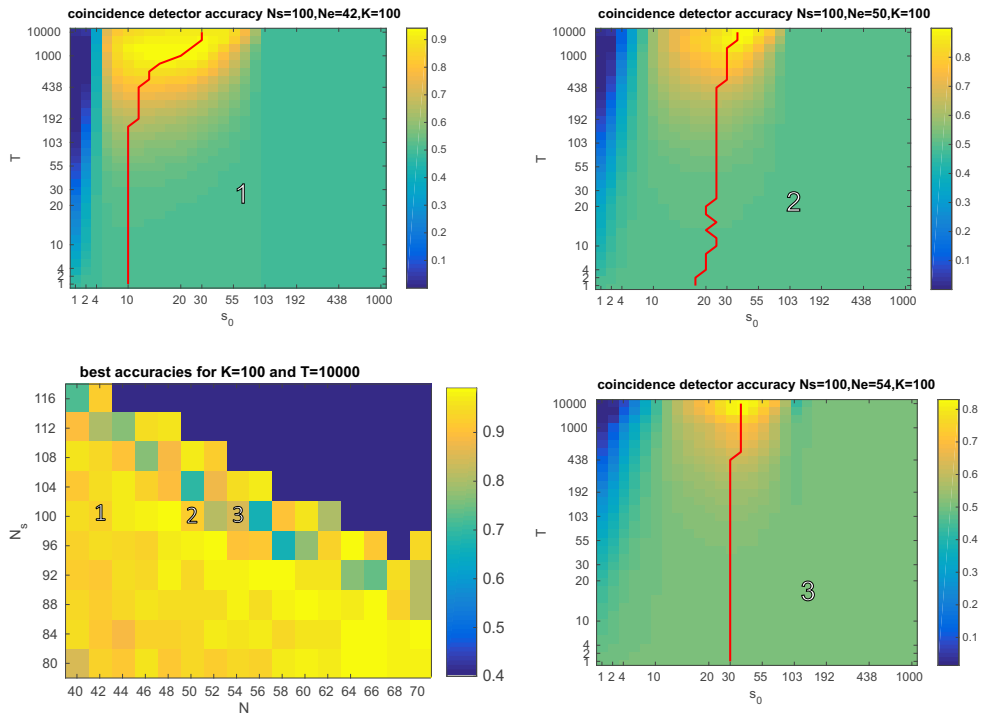


Figure 2.15: Heat plots of 2-AFC coincidence detector performance . The lower left figure shows the maximal accuracy obtainable in for the coincidence detectors with time horizon $T = 10000$. The dependency of the coincidence detector performance of the parameters T, s_0 is shown in the panels 1-3. For each parameter value T there is an optimal s_0 maximizing the accuracy in the 2-AFC task. These maximizers are connected by the red lines.

Finally, we show that this robustness against changes in K and β was shown by simulating the same 2-AFC task with parameters $\beta = 2, K = 100$ and $\beta = 1, K = 200$. As expected, increasing the number of activated elements in the background decreases the maximal accuracy achievable by the coincidence detector. Lowering

2 Feature integration with critical subnetworks

the levels of inhibition we have a smaller region of phase space available where the networks are subcritical. Nevertheless the coincidence detector achieves also for this high performance scores in the 2-AFC task.

2 Feature integration with critical subnetworks

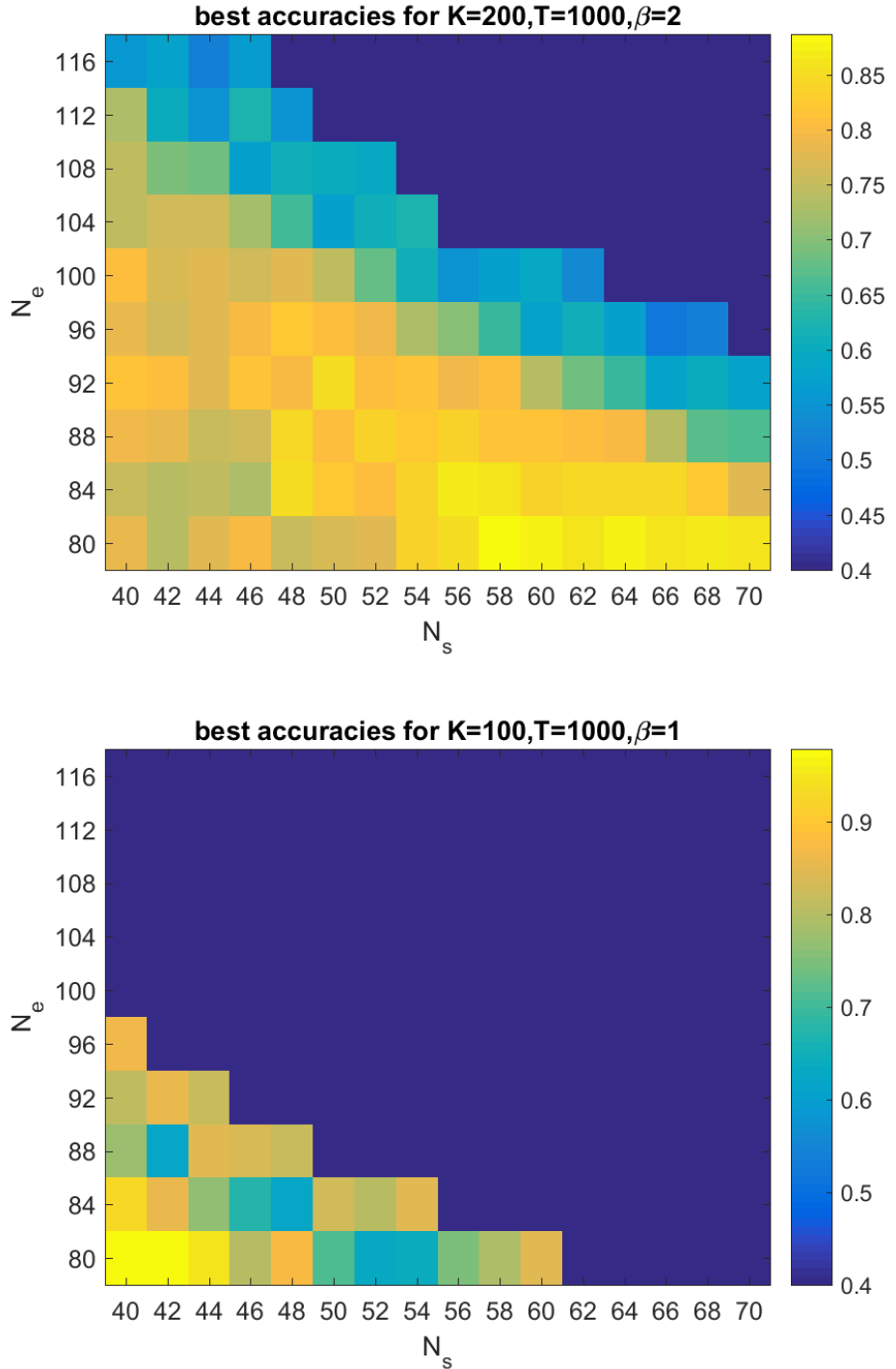


Figure 2.16: maximal accuracy of the coincidence detector for higher background noise ($K = 200$) and lower levels of inhibition ($\beta = 1$).

3 Generalized EHE model

In this chapter we extend the analytical treatment of the homogeneous EHE model given in Eurich et al. [2002], Levina [2008] to the generalized EHE model allowing for a large class of nonnegative coupling matrices W . We adopt the skew product formulation of the dynamical system using a bernoulli shift on the base to model the external input paired with a function modeling one time step of the slow time scale on the fibers (phase space) $[0, 1]^N$.

We derive the existence of a non-inhabited region where the density of states eventually vanishes, and proof that the system acts bijectively on the its complement. This that the system has an equilibrium distribution given by the uniform density supported on the complement of this non-inhabited region when paired with an uniform bernoulli measure on the base.

With the detailed understanding of the invariant phase space we show that for general nonnegative matrices the EHE model is homeomorphic to a skewed random walk on a torus.

We will carefully prove how the almost sure topological transitivity follows from the key lemma 7.3.7 in Levina [2008]. The topological transitivity paired with the uniform bernoulli measure on the base guarantees ergodicity for the homogeneous model. We conjecture that this also holds for a general class of non-constant weight matrices.

Using the (assumption) of ergodicity we construct the probability space of occurring avalanche patterns by computing the volumes of the regions leading to specific avalanches upon external input. Finally, we use this framework to rigorously derive the avalanche size statistic reported in Eurich et al. [2002].

To help the reader in following the steps, we provide a table of often used symbols with descriptions and references to the definition.

3 Generalized EHE model

Symbol	Description
N	System size
\mathcal{N}	$\{1, \dots, N\}$
e_1, \dots, e_N	Standart basis of \mathbb{R}^N
$\mathbb{1}_N$	$\sum_{i=1}^N e_i$
$[a_i, b_i)_{i \in I}$	Cylinder set 3.13
W_I	Submatrix formed of columns and rows of I
ΔU	External input strength
u	point in state space $u \in [0, 1]^N$
$\delta[\text{cond}]$	1 if cond 0 otherwise 3.4
J, I, H	Index sets with $\emptyset \neq J \subseteq I \subseteq H \subseteq \mathcal{N}$
T	EHE model as skew product dynamical system (3.1)
E_k	Function giving external input to unit k (3.2)
$A(x)$	Indicator vector for superthreshold units (3.3)
$F(x)$	Function modeling one step of the avalanche (3.5)
$k(a, u)$	number of times $F(x)$ has to be invoked until avalanche stops (3.8)
$\text{av}(a_1, u) =$	Avalanche starting at position u upon external input to u_{a_1} .
$(G_i)_{i \in \{1, \dots, D\}}$	G_i denotes the set of units firing at step i (3.9)
Ω	Set of all possible avalanche patterns av (3.10)
$\text{act}(\text{av}, i, j)$	Internal input given to unit i up to step j of avalanche av
$\Gamma(W, U, I)$	Part of non-inhabited volume generated by I (3.14)
$\Lambda(W, U, H)$	Noninhabited region along dimensions H (3.15)
\mathcal{V}	N -dimensional Volume
D	Complement of the Non-inhabited region in the phase space (3.24)
R_{av}	Region leading to avalanche pattern av 3.25

3.1 The generalized EHE-Model as a skew-product

This section outlines an approach to model the dynamics of the EHE model in the framework of dynamical systems theory, and extends the approach taken in Levina [2008].

To do so, we have to take away the stochasticity of the external input. We can do this by going from the one dimensional stochastic drive to a shift operation on the infinite dimensional sequence space. Abstracting the fast timescale avalanche dynamics in a function H (defined in 3.7), the generalized EHE model can be modeled by a skew-product dynamical system of the form

$$T : \Sigma_{\mathcal{N}}^+ \times [0, 1]^N \rightarrow \Sigma_{\mathcal{M}}^+ \times [0, 1]^N$$

$$T(a, u) = (\sigma(a), H(a, u)) . \quad (3.1)$$

$u \in [0, 1]^N, \Sigma_{\mathcal{N}}^+$ is the space of right infinite sequences $a = a_1, a_2, \dots \in \Sigma_{\mathcal{N}}^+$ over the alphabet $a_i \in \{1, \dots, N\}$ and let the measurable space of these sequences A be

3 Generalized EHE model

equipped with a probability measure ν which is the uniform bernoulli measure on $\mathcal{N} = \{1, \dots, N\}$. Each application of T represents one time step on the slow external activation timescale, with unit a_1 receiving external input and spreading of activation induced by the potentially resuling avalanche.

H can be written as composition of first handling the external input by E_{a_1} (3.2) followed by fixpoint application of F (3.5), which handles the internal input.

Let e_1, \dots, e_N denote the standard basis of R^N . To handle the external input, the coordinate of the unit receiving external input is increased by ΔU .

$$E_k(u) := u + e_k \Delta U \quad (3.2)$$

We define $A(x)$ to be vector indicating which units are above the threshold

$$A(x) := (\delta[x_i \geq 1])_{i=1, \dots, N}, \quad (3.3)$$

where

$$\delta[\text{cond}] = \begin{cases} 1 & \text{if cond} \\ 0 & \text{otherwise.} \end{cases} \quad (3.4)$$

Using this indicator vector A , the procedure to reset the spiking units and to distribute internal activation in the network is described by

$$F(x) := x - A(x) + WA(x). \quad (3.5)$$

In this chapter we analyze the dynamical system in the regime where avalanche sizes are bounded by N and each unit can fire at most once in an avalanche. As shown in proposition 3.1.1, this is ensured by the assumptions $W \geq 0$ componentwise and $W \sum_{i=1}^N e_i + \Delta U < 1$. Additionally we require $1 - 2W \sum_{i=1}^N e_i \geq 0$.

Assumptions: Throughout this chapter we restrict the analysis to the class of weight matrices W satisfying

$$W \geq 0, W \sum_{i=1}^N e_i + \Delta U < 1, 1 - 2W \sum_{i=1}^N e_i \geq 0 \text{ componentwise.} \quad (3.6)$$

We now define $H(a, u)$ modeling one step on the slow timescale by first giving external input to the system with the function E_{a_1} followed by distributing internal activation with F until no unit is above threshold.

$$H(a, u) := F^{k(a_1, u)} \circ E_{a_1}(u), \quad (3.7)$$

3 Generalized EHE model

where

$$k(a_1, u) := \min_{k \in \mathbb{N}_{\geq 0}} F^k \circ E_{a_1}(u) \in [0, 1]^N. \quad (3.8)$$

When $k(a_1, u) > 0$ we say that an avalanche occurs in the system. The function $\text{av}(a_1, u)$ returns the avalanche resulting by application of $H(a_1, u)$ and is defined by

$$\begin{aligned} \text{av}(a_1, u) &:= (G_i)_{i=1, \dots, k(a, x)} \\ G_i &= \{j \in \mathcal{N} \mid A_j(F^{i-1} \circ E_{a_1}(u)) = 1\}. \end{aligned} \quad (3.9)$$

G_i denotes the set of indices that fired during step i . When no avalanche occurs $\text{av}(a_1, u)$ is given by the empty sequence $\text{av}(a_1, u) = ()$. Since an avalanche is started always by the external input pushing exactly one unit above the threshold we have $\text{av}(a_1, u)_1 = \{a_1\}$.

Proposition 3.1.1. *If $\sum_{j=1}^N w_{ij} + \Delta U < 1$ for all $i = 1, \dots, N$, $k(a, u) \leq N$ and each unit can fire at most once during an avalanche and we have for $\text{av}(a_1, u) = (G_i)_{i=1, \dots, k(a, x)}$ that*

$$\biguplus_{i=1}^{k(a, u)} G_i \subseteq N.$$

Proof. We will give a proof by contradiction. Let $u \in [0, 1]^N$, $a_1 \in \mathcal{N}$ be arbitrary and let j be a unit that spiked twice during an avalanche at steps s_1 and s_2 and no other unit spiked twice before step s_2 . It follows that $A_j(F^{l-1} \circ E_{a_1}(u)) = 1$ for $l \in \{s_1, s_2\}$. But since no other unit spiked twice before s_2 , it also follows that

$$\begin{aligned} F^{s_2-1}(E_{a_1}(u))_j &= E_{a_1}(u)_j + (W \sum_{l=1}^{s_2} A(F^{l-1} \circ E_{a_1}(u)))_j - 1 \\ &\leq E_{a_1}(u)_j - 1 + \sum_{l=1}^N w_{jl} \leq \Delta U + \sum_{l=1}^N w_{jl} < 1, \end{aligned}$$

which contradicts $A_j(F^{s_2-1} \circ E_{a_1}(u)) = 1$. This shows that every unit can spike at most once during an avalanche and using (3.9) we have that the G_i are pairwise disjoint. $k(a_1, u) \leq N$ follows immediately. \square

This Proposition ensures that the set of avalanches in a network of N units is finite. We denote this set by Ω :

$$\Omega := \left\{ (G_i)_{i=1 \dots D} \mid \emptyset \neq G_i \subseteq \mathcal{N} \forall i \in \{1 \dots D\}, \biguplus_{i=1}^D G_i \subseteq \mathcal{N}, |G_1| \leq 1, D \geq 0 \right\} \quad (3.10)$$

We introduce two auxillary functions to shorten the following derivations in this chapter:

3 Generalized EHE model

ter. \mathcal{U} represents the set of units firing in the avalanche.

$$\begin{aligned}\mathcal{U}((G_i)_{i=1,\dots,D}, s, e) &:= \biguplus_{i=s}^e G_i \\ \mathcal{U}((G_i)_{i=1,\dots,D}) &:= \mathcal{U}((G_i)_{i=1,\dots,D}, 1, D)\end{aligned}\quad (3.11)$$

$\text{act}(\text{av}, i, j)$ is the internal input (activation) given to unit i up to step j of the avalanche av .

$$\text{act}(\text{av}, i, j) := \sum_{k=1}^{j-1} \sum_{l \in G_k} w_{il} \quad (3.12)$$

Lemma 3.1.2. *Let $\text{av} = \text{av}(a_1, u) = (G_i)_{i=1,\dots,D}$. Then*

$$(F^{j-1} \circ E_{a_1}(u))_i - E_{a_1}(u)_i = \text{act}(\text{av}, i, j) - \delta[i \in \mathcal{U}(\text{av}, 1, j-1)] .$$

Proof. If $i \in \mathcal{U}(\text{av}, 1, j-1) = \biguplus_{k=1}^{j-1} G_k$, then from (3.9) we have

$$\begin{aligned}(F^{j-1} \circ E_{a_1}(u))_i &= E_{a_1}(u) - 1 + \sum_{k=1}^{j-1} WA(F^{k-1} \circ E_{a_1}(u))_i \\ &= E_{a_1}(u) - 1 + \sum_{k=1}^{j-1} \sum_{l \in G_k} w_{il} .\end{aligned}$$

Similarly, if $i \notin \biguplus_{k=1}^{j-1} G_k$, $(F^{j-1} \circ E_{a_1}(u))_i = E_{a_1}(u) + \sum_{k=1}^{j-1} \sum_{l \in G_k} w_{il}$, which proves the statement. \square

3.2 Non-inhabited region of phase space

The following considerations show that an invariant measure can't have the whole phase space $[0, 1]^N$ as support and that there is a *non-inhabited region* which can not be entered by the dynamical system:

Suppose that unit u_i starts an avalanche in which the units in $I \subseteq \mathcal{N}$ fire, i.e $\text{av} = (G_i)_{i=1,\dots,D}, G_1 = \{i\}, \mathcal{U}(\text{av}) = I$. The coordinate of unit u_i after the avalanche stopped can not be smaller than the total input it received during the avalanche. Applying this reasoning for each possible starting unit $u_j, j \in I$ for avalanches with $\mathcal{U}(\text{av}) = I$ identifies a hyperrectangle which can never be entered by the dynamical system, i.e every point in the hyperrectangle has no preimage under T . This statement will be proven later in theorem 3.4.3.

We start by describing this region of phase space as a union of all the noninhabited regions generated by the nonempty subsets I . In the following, $\emptyset \neq J \subseteq I \subseteq H \subseteq \mathcal{N}$

3 Generalized EHE model

denote index sets. We introduce the following notation for cylinder sets:

$$[a_i, b_i)_{i \in K} := \left\{ x \in [0, 1]^N \mid a_i \leq x_i < b_i \text{ for all } i \in I \right\} \quad (3.13)$$

The part of the non-inhabited Region generated by I is defined by

$$\Gamma(W, I) := \left[0, \sum_{j \in I} w_{ij} \right]_{i \in I}. \quad (3.14)$$

The total non-inhabited region along the dimensions H is the union of the non-inhabited regions generated by all the possible subsets $\emptyset \neq I \subseteq H$

$$\Lambda(W, H) := \bigcup_{\emptyset \neq I \subseteq H} \Gamma(W, I). \quad (3.15)$$

Note that $\Lambda(W, \emptyset) = \emptyset$. See figures 3.1 and 3.2 for Illustrations of the non-inhabited regions in 2 and 3 dimensions formed by the union of overlapping Γ sets.

Given in this form, the volume of $\Lambda(W, H)$, for $H \subseteq \mathcal{N}$, is not easy to calculate by inclusion-exclusion. Fortunately, there are self-similarities in this region that can be used to derive a recursive decomposition into non-overlapping regions. Based on this decomposition it is possible to derive a closed form for the volume of the non-inhabited phase space.

The strategy to arrive at the recursive decomposition consists of three steps:

1. Perform a suitable decomposition of the state space by disjoint hyperrectangles.
2. Observe that the union of Γ intersecting such a hyperrectangle form a lower dimensional non-inhabited volume.
3. Write $\Lambda(W, H)$ as a disjoint union of these lower dimensional non-inhabited volumes.

3.2.1 Decomposition of the Phase space by disjoint hyperrectangles

In figure 3.2 one can see the self-similar structure of the noninhabited volume. The faces of the cube with $u_i = 1, i \in \{1, 2, 3\}$ each display a two dimensional non-inhabited volume while there is additional structure found at the origin ($\Gamma(W, \{1, 2, 3\})$). We make this observed self-similarity concrete by decomposing the phase space into non-overlapping hyperrectangles and showing the self-similarities in the intersections.

3 Generalized EHE model

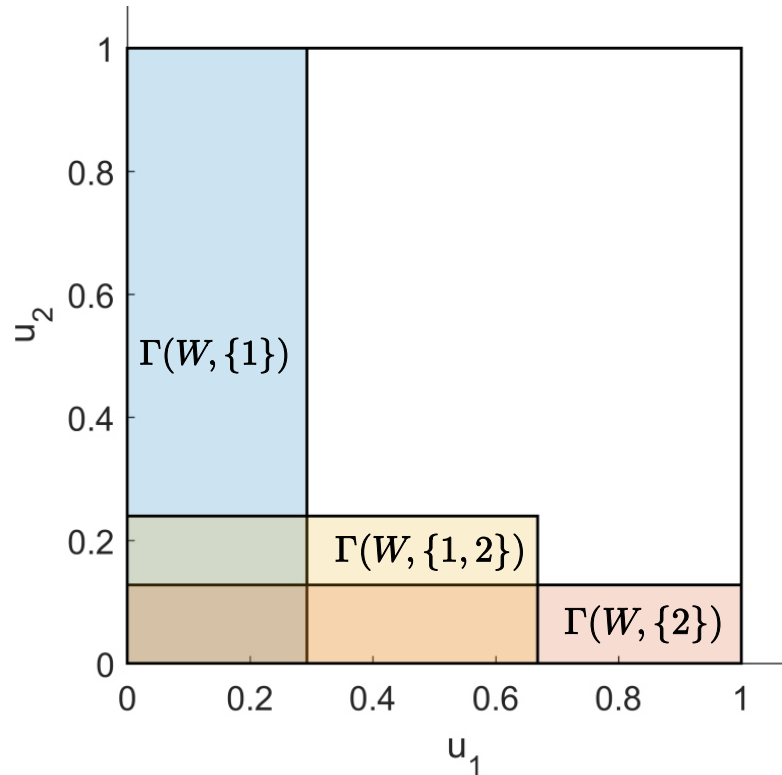


Figure 3.1: Non-inhabited region for the 2-dimensional EHE model formed by the union of non-inhabited regions generated by the subsets of units $\emptyset \neq I \subseteq \{1, 2\}$. If the coordinate u_1 is set above the threshold by the external input E_1 , action of F resets the activation value by subtracting 1, but also adding the internal activation given by $w_{1,1}$. It follows that the new state vector of the system has $u_1 \geq w_{1,1}$. u_1 not only gives internal activation to itself but also to u_2 of size w_{21} . Should this in turn cause u_2 to fire, u_1 receives the additional activation w_{12} so that the new system state can't be inside of $\Gamma(W, \{1, 2\})$.

3 Generalized EHE model

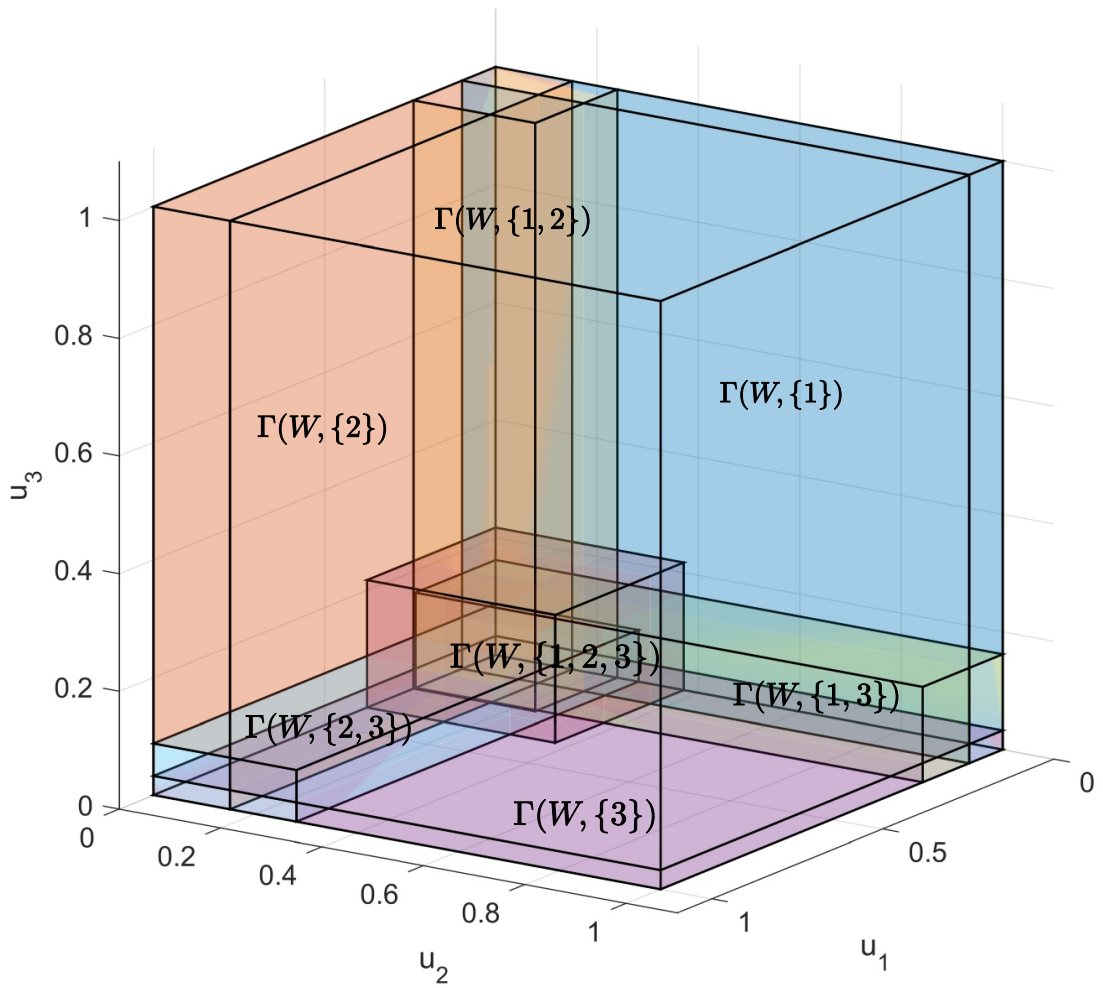


Figure 3.2: Illustration Non-inhabited region for the 3-dimensional EHE model formed by the union of non-inhabited regions generated by $\emptyset \neq I \subseteq \mathcal{N}$.

3 Generalized EHE model

We introduce the decomposition

$$[0, U_i]_{i \in H} = \bigcup_{I \subseteq H} R(W, H, I), \quad (3.16)$$

with

$$R(W, H, I) = \left[0, \sum_{j \in H} w_{ij} \right]_{i \in I} \cap \left[\sum_{l \in H} w_{kl}, 1 \right]_{k \in H \setminus I}. \quad (3.17)$$

This decomposition corresponds to the following expansion for the volume of the phase space:

$$\mathcal{V}([0, U_i]_{i \in H}) = \prod_{i \in H} U_i = \prod_{i \in H} \left(\sum_{j \in H} w_{ij} + (U_i - \sum_{j \in H} w_{ij}) \right). \quad (3.18)$$

See figure 3.3 for visualizations of these hyperrectangles for $\mathcal{N} = 3$.

3.2.2 Self similarity of the non-inhabited volume

Figure 3.3 graphically suggest that The overlap between a $R(W, H, I)$ and $\Lambda(W, H)$ is given by the overlap between $R(W, H, I)$ and the non-inhabitated region along the dimensions I .

Lemma 3.2.1. *For $\emptyset \subseteq I \subseteq H \subseteq \mathcal{N}$ we have*

$$R(W, H, I) \cap \Lambda(W, H) = R(W, H, I) \cap \Lambda(W, I). \quad (3.19)$$

Proof. Note that by definition $\Lambda(W, H) = \bigcup_{\emptyset \neq I \subseteq H} \Gamma(W, I)$. The result follows if $R(W, H, I) \cap \Gamma(W, J) = \emptyset$ for all $\emptyset \neq J \subseteq H \setminus I$.

$$R(W, H, I) \cap \Gamma(W, J) = \left[0, \sum_{j \in H} w_{ij} \right]_{i \in I} \cap \left[\sum_{l \in H} w_{kl}, 1 \right]_{k \in H \setminus I} \cap \left[0, \sum_{j \in J} w_{ij} \right]_{i \in J} = \emptyset,$$

because the intersection along $j \in J \cap (H \setminus I)$ is empty. \square

3.2.3 Recursive Decomposition of the non-inhabited region

Using the results from the previous steps, the non-inhabited region can be recursively decomposed into disjoint subsets.

Theorem 3.2.2. *For $W \geq 0, \sum_{j \in \mathcal{N}} w_{ij} + \Delta U \leq 1$ for all $i \in \mathcal{N}, \emptyset \neq H \subseteq \mathcal{N}$ and*

3 Generalized EHE model

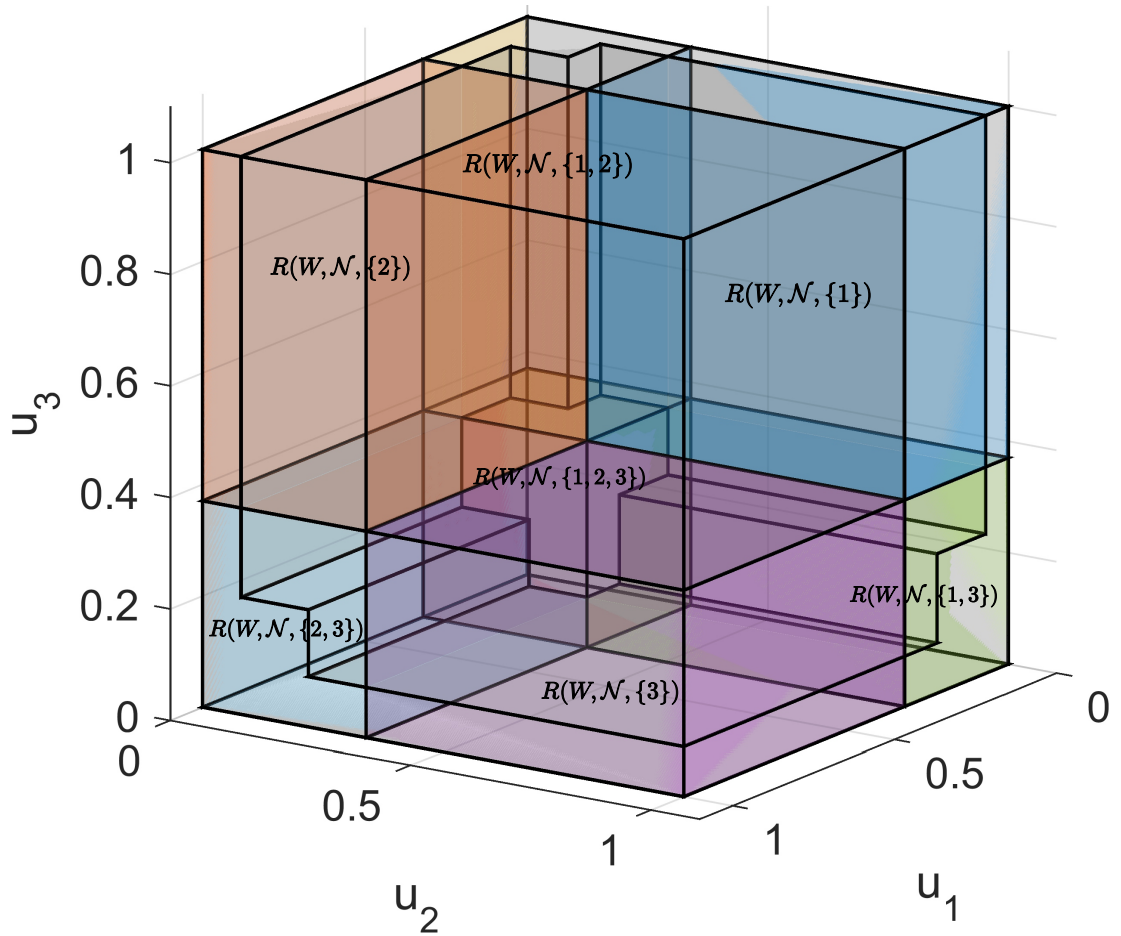


Figure 3.3: Decomposition of $[0, 1]^3$ into the non-overlapping rectangles. $R(W, \mathcal{N}, I)$ contains the non-inhabited region generated by I .

3 Generalized EHE model

$U = (U_i)_{i \in H}, \sum_{j \in H} w_{ij} \leq U_i \leq 1$ for all $i \in H$ we have

$$\Lambda(W, H) \cap [0, U_i]_{i \in H} = \biguplus_{\emptyset \neq I \subseteq H} \Lambda(W, I) \cap \left[0, \sum_{j \in H} w_{ij} \right]_{i \in H} \cap \left[\sum_{l \in H} w_{kl}, U_k \right]_{k \in H \setminus I}. \quad (3.20)$$

Proof.

$$\begin{aligned} \Lambda(W, H) \cap [0, U_i]_{i \in H} &= \biguplus_{\emptyset \neq I \subseteq H} R(W, H, I) \cap \Lambda(W, H) \cap [0, U_i]_{i \in H} \\ &= \biguplus_{\emptyset \neq I \subseteq H} R(W, H, I) \cap \Lambda(W, I) \cap [0, U_i]_{i \in H} \\ &= \biguplus_{\emptyset \neq I \subseteq H} \Lambda(W, I) \cap \left[0, \sum_{j \in H} w_{ij} \right]_{i \in I} \cap \left[\sum_{l \in H} w_{kl}, U_k \right]_{k \in H \setminus I}, \end{aligned}$$

where we used Lemma 3.2.1 for the second step and (3.17) as well as $\sum_{j \in H} w_{ij} \leq U_i \leq 1$ in the last step. \square

Theorem 3.2.2 provides the direct generalization of [Eurich et al., 2002, Equation B5] for non-negative weight matrices.

3.2.4 Volume of the non-inhabited region

With equation 3.20 one can directly compute the volume of the non-inhabited region generated by H by recursively computing all volumes of non-inhabited generated by all nonempty subsets of H . However with this formula it is not clear in what way the volume of the non-inhabited region depends on properties of W . However, it turns out that this volume does depend in a very structured way on the weight matrix: It is an alternating sum of determinants of submatrices:

Theorem 3.2.3. *Under the same assumptions as in 3.2.2 we have*

$$\mathcal{V}(\Lambda(W, H) \cap [0, U_i]_{i \in H}) = \sum_{\emptyset \neq I \subseteq H} (-1)^{|I|+1} |W_I| \prod_{j \in H \setminus I} U_j. \quad (3.21)$$

Proof. We give a proof by induction on the cardinality $|H|$.

Induction Start:

For $H = \{i\}$ we have

$$\Lambda(W, \{i\}) \cap [0, U_i]_{\{i\}} = \Gamma(W, \{i\}) \cap [0, U_i]_{\{i\}} = [0, w_{ii}]_{\{i\}} \cap [0, U_i]_{\{i\}} = [0, w_{ii}]_{\{i\}},$$

3 Generalized EHE model

and thus $\text{Vol}(\Lambda(W, \{i\}) \cap [0, U_i]_{\{i\}}) = w_{ii}$, which is equal to the right hand side of (3.21).

Inductive step:

Let (3.21) hold for all $\emptyset \neq I \subseteq \mathcal{N}$ with cardinality $|I| \leq n$. We show that it also holds for all $H \subseteq \mathcal{N}$ of cardinality $|H| = n + 1$.

We have $R(W, H, H) = \Gamma(W, H)$ and thus $R(W, H, H) \cap \Lambda(W, H) = R(W, H, H)$. Using this and inserting the induction hypothesis in each lower dimensional $\Lambda(W, I) \cap [0, U_i]_{i \in I}$ with $I \subsetneq H$ occurring in (3.20) leads to

$$\begin{aligned} \mathcal{V}(\Lambda(W, H)) &= \prod_{k \in H} \sum_{l \in H} w_{k,l} \\ &\quad + \underbrace{\sum_{\emptyset \neq I \subsetneq H} \left(\sum_{\emptyset \neq J \subseteq I} (-1)^{|J|+1} |W_J| \prod_{k \in I \setminus J} \sum_{l \in H} w_{k,l} \right)}_{\text{Ind}} \prod_{k \in H \setminus I} \left(U_k - \sum_{l \in H} w_{k,l} \right). \end{aligned} \quad (3.22)$$

We expand the term Ind into a linear combination of terms

$$F_{I', J', K'} = (-1)^{|J'|+1} |W_{J'}| \prod_{i \in I'} \sum_{j \in H} w_{i,j} \prod_{k \in K'} U_k$$

for $I' \uplus J' \uplus K' = H, J' \subsetneq H$:

$$\text{Ind} = \sum_{I' \uplus J' \uplus K' = H, J' \subsetneq H} C_F(I', J', K') (-1)^{|J'|+1} |W_{J', J'}| \prod_{i \in I'} \sum_{j \in H} w_{i,j} \prod_{k \in K'} U_k$$

In order to calculate $C_F(I', J', K')$ we use that $F_{I', J', K'}$ only occurs in (3.22) for the assignments $J = J'$ and $I' = J' \uplus I$ and perform a case analysis:

- $I' = \emptyset, K' = H \setminus J'$: $C_F(\emptyset, J', H \setminus J') = 1$, since with $I' = \emptyset$ there is only one assignment $I = J = J'$ in (3.22) resulting in $F_{\emptyset, J', H \setminus J'}$.
- $K' = \emptyset, I' = H \setminus J'$: $C_F(N \setminus J, J', \emptyset) = -1$. The $\prod_{i \in I'} \sum_{j \in H} w_{i,j}$ terms can originate from any $J = J', J' \subseteq I \subsetneq H$ combined with the $\prod_{k \in H \setminus I} - \sum_{l \in H} w_{k,l}$ term. The sign of this term is given by $(-1)^{|H \setminus I|}$. Counting the possible ways to choose i' elements from I' and the signs of the resulting combinations we arrive at

$$C_F(N \setminus J, J', \emptyset) = \sum_{i'=1}^{|I'|} (-1)^{|I'| - i'} \binom{|I'|}{i'} = -1.$$

3 Generalized EHE model

- $I' \neq \emptyset, K' \neq \emptyset$: $C_F(I', J', K') = 0$. As in the previous case, the $\prod_{i \in I'} \sum_{j \in H} w_{i,j}$ terms can be formed from any completion $J' \subseteq I \subseteq J' \uplus K'$, with the difference that now also $I = I'$ can be chosen. This results in

$$C_F(I', J', K') = \sum_{i'=0}^{|I'|} (-1)^{|I'| - i'} \binom{|I'|}{i'} = 0 .$$

Setting this into (3.22) gives

$$\begin{aligned} \mathcal{V}(\Lambda(W, H)) &= \sum_{\emptyset \neq I \subsetneq H} (-1)^{|I|-1} |W_{I,I}| \prod_{k \in H \setminus I} U_k \\ &\quad + \underbrace{\sum_{\emptyset \neq J \subsetneq H} (-1)^{|J|} |W_{J,J}| \prod_{k \in H \setminus J} \sum_{l \in H} w_{k,l} + \prod_{m \in H} \sum_{n \in H} w_{m,n}}_T . \end{aligned}$$

The left term alone contains all lower dimensional determinant terms needed in (3.21). We complete the proof by showing that

$$T = (-1)^{|H|+1} |W_H| . \quad (3.23)$$

The expansion of the third term contains all $|H|^{|H|}$ products of matrix elements $\prod_{i \in H} w_{i,\sigma(i)}$ where $\sigma(i)$ is a function from H to H , while $(-1)^{|H|+1} |W_H|$ can be expanded using the Leibniz formula

$$(-1)^{|H|+1} |W_H| = \sum_{\varphi} (-1)^{|H|-1} \text{sign}(\varphi) \prod_{i \in H} w_{i,\varphi(i)},$$

where the sum is performed over all permutations of H .

To show the equality in (3.23) we again expand T into a linear combination of the terms $T_\sigma = \prod_{i \in H} w_{i,\sigma(i)}$ for the $|H|^{|H|}$ functions $\sigma : H \rightarrow H$ with coefficients C_σ

$$T = \sum_{\sigma} C_\sigma \prod_{i \in H} w_{i,\sigma(i)} .$$

The term

$$(-1)^{|J|} |W_J| \prod_{k \in H \setminus J} \sum_{l \in H} w_{k,l} = \sum_{\sigma} C_\sigma^J \prod_{i \in H} w_{i,\sigma(i)}$$

3 Generalized EHE model

contains just the terms corresponding to functions σ for which $\sigma|_J$ is a permutation, so we have

$$C_\sigma^J = \delta[\sigma|_J \text{ is a permutation of } J](-1)^{|J| + \text{sign}(\sigma|_J)}$$

$$\text{and } C_\sigma = \sum_{\emptyset \neq J \subsetneq H} C_\sigma^J + 1.$$

In order to calculate C_σ for a given function σ , we introduce the set

$$\begin{aligned} Z^\sigma = \{Z \subset H | & \sigma|_Z \text{ is a permutation of } Z \\ & \text{and there is no } Z' \subset Z \text{ such that} \\ & \sigma|_{Z'} \text{ is a permutation of } Z'\} . \end{aligned}$$

For a permutation, this is just the set of cycles and more generally when viewing a function σ as markov chain, Z^σ are its transitive components.

For a subset \mathcal{Z} of Z^σ we introduce $\mathcal{U}(\mathcal{Z}) = \bigcup_{Z_i \in \mathcal{Z}} Z_i$. We now have that $\sigma|_J$ is a permutation of J if and only if $J = U(\mathcal{Z})$ for a $\emptyset \neq \mathcal{Z} \subseteq Z^\sigma$. We have $\mathcal{U}(Z^\sigma) = H$ if and only if σ is a permutation of H .

We now have for $\emptyset \neq \mathcal{U}(\mathcal{Z}) \subsetneq H$

$$\begin{aligned} C_\sigma^{\mathcal{U}(\mathcal{Z})} &= (-1)^{|\mathcal{U}(\mathcal{Z})|} \text{sign}(\sigma|_{\mathcal{U}(\mathcal{Z})}) \\ &= (-1)^{|\mathcal{U}(\mathcal{Z})| + \sum_{Z \in \mathcal{Z}} (|Z|-1)} \\ &= (-1)^{2|\mathcal{U}(\mathcal{Z})| - |\mathcal{Z}|} = (-1)^{|\mathcal{Z}|} , \end{aligned}$$

and

$$\begin{aligned} C_\sigma &= 1 + \sum_{\emptyset \neq J \subsetneq H} C_\sigma^J = 1 + \sum_{\emptyset \neq \mathcal{Z} \subseteq Z^\sigma, \mathcal{U}(\mathcal{Z}) \subsetneq H} C_\sigma^{\mathcal{U}(\mathcal{Z})} \\ &= 1 + \sum_{\emptyset \neq \mathcal{Z} \subseteq Z^\sigma, \mathcal{U}(\mathcal{Z}) \subsetneq H} (-1)^{|\mathcal{Z}|} = \sum_{z=0}^{|Z^\sigma|-1} \binom{|Z^\sigma|}{z} (-1)^z + \delta[\mathcal{U}(Z^\sigma) \subsetneq H](-1)^{|Z^\sigma|} \\ &= \begin{cases} (-1)^{|Z^\sigma|-1} & \text{if } \sigma \text{ is a permutation of } H \\ 0 & \text{otherwise} . \end{cases} \end{aligned}$$

This completes the proof since for a permutation φ of H $(-1)^{|H|-1} \text{sign}(\varphi) =$

3 Generalized EHE model

$(-1)^{|H|-1+|H|-|Z^\varphi|} = (-1)^{|Z^\varphi|-1}$ and by comparing the coefficients we have

$$T = \sum_{\sigma} C_{\sigma} \prod_{i \in H} w_{i, \sigma(i)} = (-1)^{|H|+1} |W_H| .$$

□

3.3 Identification of regions leading to avalanches

We introduce the shorthand

$$D := [0, 1]^N \setminus \Lambda(W, \mathcal{N}) \quad (3.24)$$

for the complement of the non-inhabited region.

Before we proceed to show that the complement of the non-inhabited region is invariant under T we identify the regions $R(W, (G_i)_{i=1, \dots, D}) \subseteq D$. For $u \in R(W, (G_i)_{i=1, \dots, D})$, with $G_1 = \{a_1\}$ external input to unit u_{a_1} produces the avalanche $\text{av}(a_1, u) = (G_i)_{i=1, \dots, D}$.

The coordinate of unit u_{a_1} , which receives the external input and starts the avalanche has to be in the interval $[1 - \Delta U, 1)$. The coordinates of the units in $G_j, 1 < j \leq D$ have to be such that the total internal input generated during the avalanche up to step $j - 1$ did not cause them to spike, but the additional internal input generated by step $j - 1$ is enough to push them above the threshold. For the coordinates along the axis not occurring in av , the condition is that the total input generated from the whole avalanche is not enough to make them spike and that they lie outside of the non-inhabited area.

This reasoning specifies $R(W, \text{av})$, $\text{av} = (G_i)_{i=1, \dots, D}, G_1 = \{a_1\}$ as

$$\begin{aligned} R(W, \text{av}) &= [1 - \Delta U, 1)_{\{a_1\}} \bigcap_{j=2}^D [1 - \text{act}(\text{av}, k, j), 1 - \text{act}(\text{av}, k, j - 1))_{k \in G_j} \\ &\cap ([0, 1 - \text{act}(\text{av}, l, D)]_{l \in \mathcal{N} \setminus \mathcal{U}(\text{av})} \setminus \Lambda(W, \mathcal{N} \setminus \mathcal{U}(\text{av}))) . \end{aligned} \quad (3.25)$$

Theorem 3.3.1. For $(G_i)_{i=1, \dots, D} \in \Omega, 1 \leq D \leq N$

$$R(W, (G_i)_{i=1, \dots, D}) = \{u \in D \mid \text{av}(u, a_1) = (G_i)_{i=1, \dots, D}, G_1 = \{a_1\}\}$$

Proof. We will list the conditions on $u \in D$ so that it generates the nonempty avalanche $\text{av} = (G_i)_{i=1, \dots, D}$ upon external activation of unit $\{a_1\} = G_1$.

3 Generalized EHE model

Since $G_1 = \{a_1\}$, it follows that

$$A(E_{a_1}(u))_{a_1} = 1 \iff u_{a_1} + \Delta U \geq 1 \iff u_{a_1} \in [1 - \Delta U, 1] .$$

Using theorem 3.1.1, the condition that unit k spikes only in step j in the avalanche, $k \in G_j$ reduces to $A(F^{j-1} \circ E_{a_1}(u))_k = 1$, and we have

$$(F^{j-1} \circ E_{a_1}(u))_k \geq 1 > (F^{j-2} \circ E_{a_1}(u))_k .$$

Performing the iterations of F using lemma 3.1.2 and observing that $E_{a_1}(u)_k = u_k$, this condition reduces to

$$\begin{aligned} u_k + \text{act(av, } k, j) &\geq 1 > u_k + \text{act(av, } k, j-1) \iff \\ u_k &\in [1 - \text{act(av, } k, j), 1 - \text{act(av, } k, j-1)) . \end{aligned}$$

If unit $l \in [0, 1] \setminus \Lambda^{\mathcal{N}}(W, 1)$ does not fire during av, $l \notin \mathcal{U}(\text{av})$, then $A(F^{i-1} \circ E_{a_1}(u))_l = 0$ for all $i = 1, \dots, D$. This restricts each u_l to the interval $u_l \in [0, 1 - \text{act(av, } l, D))$.

We now only have to satisfy the condition that $u \in D = [0, 1]^N \setminus \Lambda(W, \mathcal{N})$. We have with (3.6)

$$\begin{aligned} [1 - \Delta U, 1]_{\{a_1\}} \bigcap_{j=2}^D [1 - \text{act(av, } k, j), 1 - \text{act(av, } k, j-1))_{k \in G_j} \cap \Lambda(W, \mathcal{N}) &= \\ [1 - \Delta U, 1]_{\{a_1\}} \bigcap_{j=2}^D [1 - \text{act(av, } k, j), 1 - \text{act(av, } k, j-1))_{k \in G_j} \cap \Lambda(W, \mathcal{N} \setminus \mathcal{U}) , \end{aligned}$$

since $1 - \text{act(av, } k, j) \geq \sum_{l \in \mathcal{N}} w_{kl}$. □

3.4 T acts bijectively on D

Let π_D denote the projection to D . We are now proceeding to show that $\pi_D(T(a_1, \cdot))$ with $a_1 \in \mathcal{N}$ has the complement of the non-inhabited region as invariant set and acts bijectively on it. For all points $u \in D \setminus \bigcup_{\text{av} \in \Omega, \text{av} \neq ()} R(W, \text{av})$ this is trivially true since on this region $T(a_1, \cdot)$ is just a shift in the direction e_{a_1} of length ΔU which does not leave D , since it starts no avalanche.

What remains to be shown is that the Images of the regions R_{av} are in the complement of the non-inhabited region and that they are pairwise disjoint. We will show that in a constructive way by constructing all images of the regions $R(W, \text{av})$. We use $S + v$ for a set S and a vector v as shorthand for the set $\{s + v | s \in S\}$.

Proposition 3.4.1. *For $() \neq \text{av} \in \Omega, a_1 \in \mathcal{N}$ the image $\pi_D(T_{a_1}, R(W, \text{av}))$ of*

3 Generalized EHE model

$R(W, \text{av})$ under $T(a_1, \cdot)$ is given by

$$\begin{aligned} & \left[\sum_{j \in \mathcal{U}(\text{av})} w_{ij}, \sum_{j \in \mathcal{U}(\text{av})} w_{ij} + \Delta U \right]_{G_1} \cap \\ & \bigcap_{j=2, \dots, D} \left[\sum_{n \in \mathcal{U}(\text{av}, j, D)} w_{mn}, \sum_{n \in \mathcal{U}(\text{av}, j-1, D)} w_{mn} \right]_{m \in G_j} \cap \left[\sum_{n \in \mathcal{U}(\text{av}, j, D)} w_{mn}, 1 \right]_{m \in \mathcal{N} \setminus \mathcal{U}(\text{av}, 1, D)} \\ & \setminus \left(\Lambda(W, \mathcal{N} \setminus \mathcal{U}(\text{av})) + \left(\sum_{k \in \mathcal{U}(\text{av}, 1, D)} w_{lk} \right)_{l \in \mathcal{N} \setminus \mathcal{U}(\text{av})} \right) \end{aligned} \quad (3.26)$$

Proof. For $u \in R(W, \text{av})$ We have using lemma 3.1.2

$$T(a_1, u)_j = (F^{D-1} \circ E_{a_1}(u))_j = u_j + \delta_{a_1}^j \Delta U + \text{act}(\text{av}, j, D) - \delta[j \in \mathcal{U}(\text{av})]$$

so $T(a_1, \cdot)$ acts as a shift of $(\sum_{j \in \mathcal{U}(1, D)} w_{ij} + \delta[i = a_1] \Delta U - \delta[i \in \mathcal{U}(\text{av})])_{i \in \mathcal{N}}$ on $R(W, \text{av})$. \square

The injectivity of $\pi_D T(a_1, \cdot)$ on the regions $\biguplus_{\text{av} \in \Omega, \text{av}_1=\{a_1\}} R(W, \text{av})$ remains to be shown. Since on each single R_{av} , $T(a_1, \cdot)$ acts as a shift, it suffices to show that the images of different regions are pairwise disjoint.

Theorem 3.4.2. *Let $\Omega_{a_1} = \{() \neq \text{av} \in \Omega | \text{av}_1 = \{a_1\}\}$. It holds that $T(a_1, R_{\text{av}1}) \cap T(a_1, R_{\text{av}2}) = \emptyset$ for $\text{av}1, \text{av}2 \in \Omega_{a_1}, \text{av}1 \neq \text{av}2$.*

Proof. For every $\text{av}1$ we show that its image is disjoint with the images of any $\text{av}2$ with $|s'_n| = |\mathcal{U}(\text{av}2)| \leq |s_n| = |\mathcal{U}(\text{av}1)|$.

Since all $R(W, \text{av}1), R(W, \text{av}2)$ with $\text{av}1, \text{av}2 \in \Omega_{a_1}$ with the same $\mathcal{U}(\text{av}1) = \mathcal{U}(\text{av}2)$ are shifted the same amount by $T(a_1, \cdot)$, it is sufficient to show that the regions $T(a_1, s_n) = \biguplus_{\text{av} \in \Omega_{a_1}, \mathcal{U}(\text{av})=s_n} T(a_1, \text{av})$ are pairwise disjoint.

We now complete the proof by showing that $T(a_1, s_n) \cap T(a_1, s_j) = \emptyset$ for all $s_j, |s_j| \leq |s_n|$.

Let $M = s_n \setminus s_j$ be the nonempty set of indices occurring in s_n but not in s_j , and let $u^1 \in T(a_1, s_n), u^2 \in T(a_1, s_j)$ be arbitrary. Then $u_m^1 < \sum_{i \in s_n} w_{mi}$ for all $m \in M$, while

3 Generalized EHE model

$$u_m^2 \in \left[\sum_{n \in \mathcal{U}(\text{av1}, j, D)} w_{mn}, 1 \right]_{m \in \mathcal{N} \setminus \mathcal{U}(\text{av1})} \\ \setminus \left(\Lambda(W, \mathcal{N} \setminus \mathcal{U}(\text{av1})) + \left(\sum_{l \in \mathcal{U}(\text{av1})} w_{kl} \right)_{k \in \mathcal{N} \setminus \mathcal{U}(\text{av1})} \right).$$

Now since $M \subseteq \mathcal{N} \setminus \mathcal{U}(\text{av1})$ we have $\Gamma(W, M) \subseteq \Lambda(W, \mathcal{N} \setminus \mathcal{U}(\text{av1}))$ so that for the component u_m^2 it holds that $u_m^2 \geq \sum_{j \in M} w_{mj} + \sum_{l \in \mathcal{U}(\text{av1}, 1, D)} w_{ml} \geq \sum_{i \in s_n} w_{mi} > u_m^1$ which proves that the intersection is the empty set. \square

With the explicit construction of images for each av it is now easy to show that the complement of the non-inhabited region is an invariant set for the dynamical system.

Theorem 3.4.3. *For every $a_1 \in \mathcal{M}$, $\pi_X T(a_1, D) = D$*

Proof. The key step is to show that the images $\pi_D T(a_1, R(W, \text{av}))$ lie in the complement of $\Lambda(W, \mathcal{N})$. We show this by stating that for any avalanche $\text{av} = (G_i)_{i=1, \dots, D}$ with $G_1 = a_1$ and every $I \subseteq \mathcal{N}$ the intersection $\pi_D T(a_1, R(W, \text{av})) \cap \Gamma(W, I) = \emptyset$.

This is shown by a case distinction. First let $I \subseteq \mathcal{U}(\text{av})$. Let d_1 be the first step of the avalanche in which at least one unit of I spikes during the avalanche and call this unit i_1 .

Using proposition 3.4.1 and $I \subset \mathcal{U}(\text{av}, d_1, D)$ we have

$$\pi_D T(a_1, R(W, \text{av}))_{i_1} \geq \sum_{n \in \mathcal{U}(\text{av}, d_1, D)} w_{i_1 n} \geq \sum_{n \in I} w_{i_1 n},$$

while $\Gamma(W, I)_{i_1} < \sum_{n \in I} w_{i_1 n}$.

If I is no subset of $\mathcal{U}(\text{av})$ we have $I' = I \setminus \mathcal{U}(\text{av}) \neq \emptyset$. We have from 3.25 that $R(W, \text{av}) \cap \Lambda(W, I') = \emptyset$ and in particular $R(W, \text{av}) \cap \Gamma(W, I') = \emptyset$. $T(a_1, \cdot)$ acts as a shift by $s_{R_{\text{av}}} = (\sum_{j \in \mathcal{U}(1, D)} w_{ij} + \delta[i = a_1] \Delta U - \delta[i \in \mathcal{U}(\text{av})])_{i \in \mathcal{N}}$ on R_{av} . Applying this shift to $\Gamma(W, I')$ we have that

$$(\Gamma(W, I') + s_{R(W, \text{av})}) \cap \pi_D T(a_1, R(W, \text{av})) = \emptyset,$$

while $\Gamma(W, I) \subseteq \Gamma(W, I') + s_{R(W, \text{av})}$ so $\pi_D T(a_1, R(W, \text{av})) \cap \Gamma(W, I) = \emptyset$.

Up to now we have shown that $\pi_D T(a_1, D) \subseteq D$. For the other direction note that for $u \in D$ if $u_{a_1} - \Delta U \in D$ we have $T^{-1}(a_1, u) = u - e_{a_1} \Delta U$. Since every point in the section $[1 - \Delta U, 1]_{\{a_1\}}$ causes an avalanche and their images are disjoint as shown in

3 Generalized EHE model

3.4.2, every point $u \in D$ with $u - \Delta U e_{a_1}$ is part of exactly one $T(a_1, R(W, \text{av}))$ and thus has a unique preimage in D . \square

For the three dimensional case we can visualize the regions leading to avalanches and their images, as illustrated in figure 3.4.

3.4.1 Invariant measure

With this results we can proceed to show that the uniform Lebesgue measure paired with the uniform Bernoulli measure on Σ_N^+ is an invariant measure for the dynamical system.

Theorem 3.4.4. *Let μ be a uniform Bernoulli measure on Σ_M^+ and λ a Lebesgue measure on $D = [0, 1]^N \setminus \Lambda^N(W, 1)$. Then $\mu \times \lambda$ is a measure on $\Sigma_M \times D$, which is invariant under the transformation T .*

Proof. The proof follows the same line of reasoning as the corresponding proof for the original EHE model in [Levina, 2008, Theorem 7.3.1]. We have to prove that for any $a \in \Sigma_M$ and $B \subseteq D$, $(\mu \times \lambda)(a, B) = (\mu \times \lambda)(T^{-1}(a, B))$. We have that $T^{-1}(a, B) = \bigcup_{i=1}^{|M|} (g_{m_i}, B_i)$, where $M = \{m_1, m_2, \dots\}$, $g_{m_i} = \{m_i, a_1, a_2, \dots\}$ and $T(g_{m_i}, B_i) = (a, B)$. Without loss of generality consider $i = 1$. Application of the external input to unit m_1 causes either an empty avalanche or an avalanche $\text{av} \in \Omega_{m_1}$. This are the only possible choices according to Theorem 3.1.1. From Threorems and Propositions 3.3.1,3.4.1,3.4.2 we know that D can be decomposed into nonoverlapping hyperrectangles corresponding to the regions that produce the possible avalanche patterns, that on each of these regions T acts as a shift and that all the images are pairwise disjoint. Therefore, $\pi_D T(m_1, \cdot)$ preserves the measure λ . \square

3.5 The EHE Model as random walk on the N-Torus

In this section we show that the EHE Model can be written as a skewed random walk on the N-Torus. To do this, we identify ('glue together') the boundaries of the regions $R(W, (\text{av}))$ and the corresponding boundaries of their images. This is illustrated in figure 3.5. Instead of resetting after the system state crosses the boundary of D , it enters a displaced copy of D . In this way copies of D tessellate the plane and the system reduces to a random walk in the positive directions of the axes.

3 Generalized EHE model

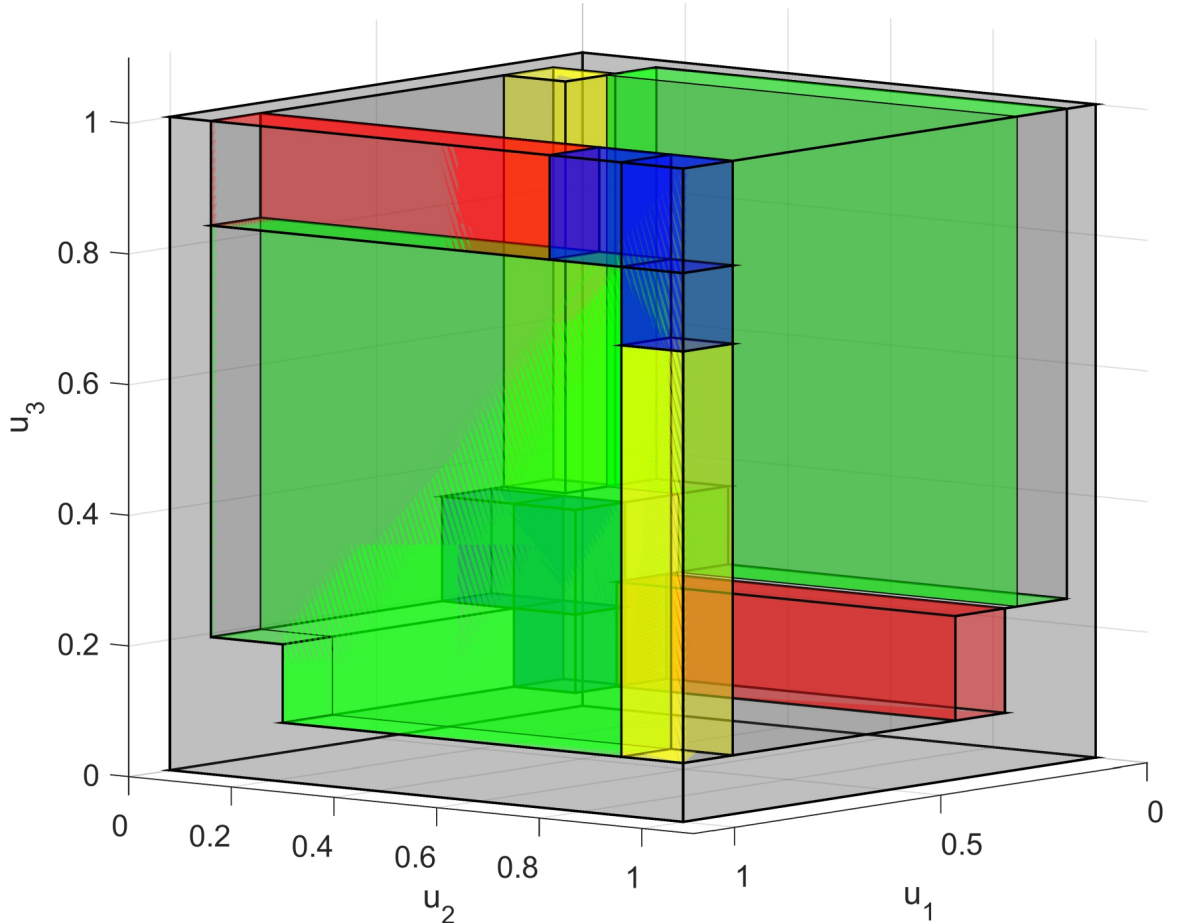


Figure 3.4: Regions leading to avalanche patterns for the three dimensional EHE System.. The green region displays $R(W, \{1\})$ and its image. The red region displays $R(W, \{1\}, \{3\})$. In this region the activation given to u_3 from u_1 is enough to make it spike itself, but the starting value of unit u_2 is low enough that it is not pushed above the threshold. The yellow region represents $R(W, \{1\}, \{2\})$, which behaves the same as the red region with the roles of u_2 and u_3 switched. The three blue regions from top left to bottom right are the regions $R(W, \{1\}, \{3\}, \{2\})$), $R(W, \{1\}, \{2, 3\})$) and $R(W, \{1\}, \{2\})$).

3 Generalized EHE model

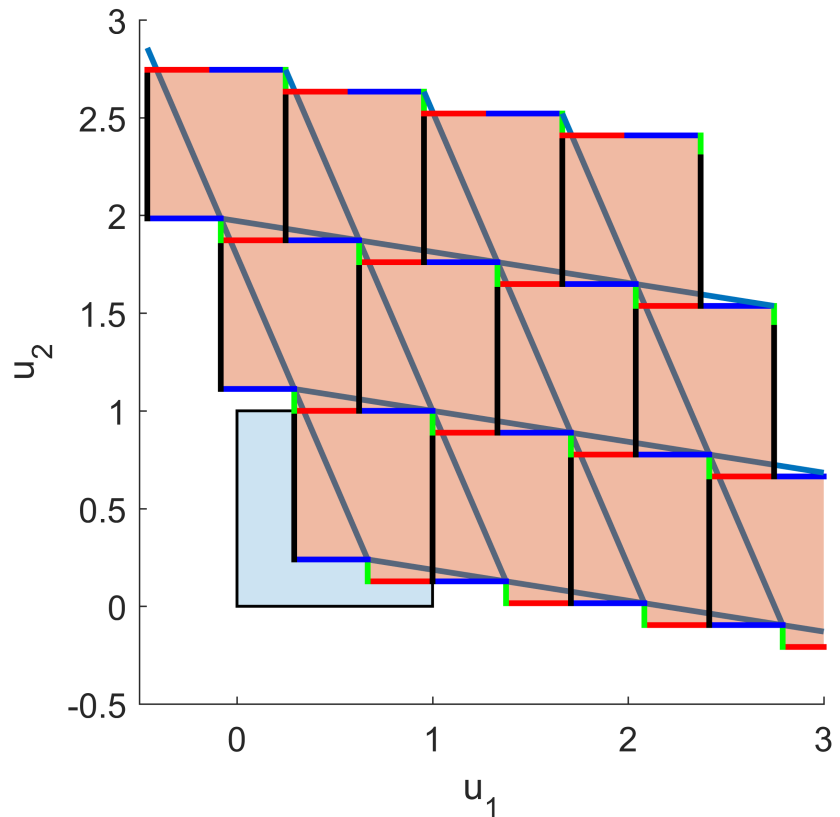


Figure 3.5: Copies of the 2 dimensional D tessellate the plane. In this tessellation, copies of D are displaced according to integer coefficients of the vectors S_1, S_2 with $S_i = (\delta[i = j] - w_{ji})_{j \in \mathcal{N}}$. This lattice induces a quotient topology in which EHE model reduces to a random walk choosing one of the directions e_1, \dots, e_N and performing a shift of ΔU in this direction.

3 Generalized EHE model

We define for $a, b \in \mathbb{R}^N$

$$a \sim_W b \text{ if and only if } a - b = \sum_{i=1}^N S_i z_i, z_i \in \mathbb{Z} \text{ for all } i = 1, \dots, N \quad (3.27)$$

$$S_i = (\delta[i=j] - w_{ji})_{j \in \mathcal{N}}.$$

In particular we show that $\pi_D T(a_1, \cdot)$ for $a_1 \in \mathcal{N}$ is just a shift by $\Delta U e_{a_1}$ with respect to this quotient topology.

This quotient space is homeomorphic to the N -torus.

Proposition 3.5.1. \mathbb{R}^N / \sim_W is homeomorphic to the N -torus for all $W \geq 0, \sum_{i=1}^N w_{ji} + \Delta U < 1$ for all $j \in \mathcal{N}$.

Proof. We have to show that $(S_i)_{i \in \mathcal{N}}$ forms a basis of \mathbb{R}^N .

Note that $S = I - W$.

The row-sum norm $\|\cdot\|_Z$ gives an upper bound on the norm of the eigenvalues of W . for $Wv = \lambda v, v \neq 0$ we have

$$|\lambda| \|v\|_\infty = \|Wv\|_\infty \leq \|W\|_Z \|v\|_\infty \implies \lambda \leq 1 - \delta U.$$

It follows that S is invertible via a Neumann series Petersen et al.. The Inverse of S provides the homeomorphism to the N -Torus. \square

Now we show that on $\mathbb{R}^N / \sim_W \pi_D T(a_1, \cdot)$ can be seen as a shift $\pi_D T(a_1, x) = x + \Delta U e_{a_1}$

Proposition 3.5.2. Let $a_1 \in \mathcal{N}$ be arbitrary and define

$$\begin{aligned} \tilde{T}(a_1, x) : \mathbb{R}^N / \sim_W &\longrightarrow \mathbb{R}^N / \sim_W \\ x &\mapsto x + \Delta U e_{a_1}. \end{aligned}$$

For $u \in D$ it holds that

$$\pi_D T(a_1, u) \sim_W \tilde{T}(a_1, u).$$

Proof. For $u_{a_1} \in [0, 1 - \Delta U]$ the statement follows trivially. Every point with $u_{a_1} \geq 1 - \Delta U$ starts an avalanche av upon external activation with a_1 and belongs to exactly

3 Generalized EHE model

one $R(W, \text{av})$. We have using Proposition 3.4.1

$$\begin{aligned}\pi_D T(a_1, u) &= u + \left(\sum_{j \in \mathcal{U}(1, D)} w_{ij} + \delta[i = a_1] \Delta U - \delta[i \in \mathcal{U}(\text{av})] \right)_{i \in \mathcal{N}} \\ &= u + \Delta U e_{a_1} - \sum_{i \in \mathcal{U}(\text{av})} S_i \sim_W u + \Delta U e_{a_1} = \tilde{T}(a_1, u).\end{aligned}$$

□

In the following we will assume T defined on \mathbb{R}^N / \sim_W and use the quotient topology. Figure 3.6 shows the 2 dimensional ehe model transformed to the torus by the inverse of S .

3.6 Topological transitivity and ergodicity of the homogeneous EHE-Model

In this section we establish the ergodicity of the homogeneous EHE-Model.

We start by citing the key Lemma in the proof of the Topological transitivity in [Levina, 2008, Chapter 7] and a careful completion of the proof using this lemma. Using this almost sure topological transitivity in the phase space we show that this implies the ergodicity of the skew-product T .

We use the notation $T^l(b, x)$ with b being a finite sequence of length at least l as shorthand for $T^l(ba, x)$ for an arbitrary $a \in \Sigma_N^+$.

The main assumptions needed for the topological transitivity are Levina [2008]

- α and δ are irrational and rationally independent
- $\alpha + \delta < 1$
- $\delta < \frac{\alpha}{N}$
- $\alpha \frac{N+1}{N} < 1$

Lemma 3.6.1 (Levina [2008]Lemma. 7.3.7). *For any $y, z \in D$ and any $\epsilon > 0$ there exists a finite sequence $b(y, z) = (b(y, z)_i)_{i=1}^{L(y, z)}$ of length $L(y, z)$, such that the euclidean distance $|z - \pi_D(T^{L(y, z)}(b(y, z), y))| < \epsilon$ and there is a uniform upper bound on $L(y, z)$ not depending on y, z , $L(y, z) \leq M(N, \epsilon, \alpha, \delta)$.*

Theorem 3.6.2 (Levina [2008]Theorem 7.3.2). *For almost all (with respect to a uniform Bernoulli measure) sequences $a \in A$, $\pi_D T(a, X)$ is topologically transitive on D .*

3 Generalized EHE model

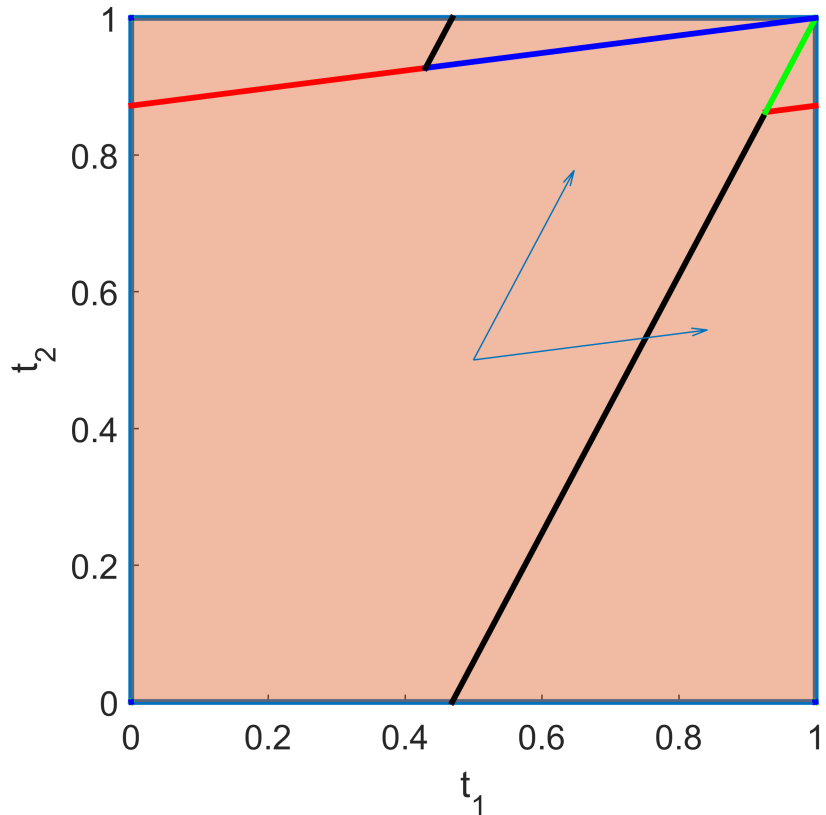


Figure 3.6: The generalized EHE-model on the torus. At each step of the model the current state is shifted by one of the two vectors. When the trajectory of the system intersects one of the lines, an avalanche is fired. The black line represents firing of just u_1 , the red line firing of just u_2 , while the green and blue lines represent avalanches involving both units. Crossing the blue Line, u_2 starts the avalanche while crossing the green line the avalanche is started by u_1 .

3 Generalized EHE model

proof extended from Levina [2008]/Page 99. We have to prove that for almost all $a \in A$ and for any open subsets $U, V \subseteq D$, there exists an $n \in \mathbb{N}$ such that $\pi_D(T^n(a, U)) \cap V \neq \emptyset$.

With [Levina, 2008, Lemma 7.3.7] we have the existence of finite sequences with uniform upper bound on their length which move any point in D to the ϵ Neighborhood of any other point in D . To complete the proof we have to show that for any two points $x \in U, z \in V$ the set of sequences eventually moving the image of x to the vicinity of z has full measure. However this alone is not enough to proof the almost sure topological transitivity since to directly use this for all open subsets U, V one would have to make an uncountable intersection of sets with probability one.

We solve this issue by constructing a sequence of regular grids on D with distance between grid points converging to zero and showing that for each pair of points g_d^i, g_e^j from grids in the sequence that the set

$$A_{g_d^i, g_e^j} := \{a \in A \mid |\pi_D(T^n(a, g_d^i)) - g_e^j| < \epsilon, \text{ for some } n \in \mathbb{N}\}$$

has full measure. Since we now have only countable many points on the sequence of grids the intersection of all $A_{g_d^i, g_e^j}$ for pairs of grid points still has probability one.

This is enough to prove the almost sure topological transitivity since for every pair of $U, V \subseteq D$ there exists a point in the grid sequence which is in U and a point in the grid sequence for which the ϵ ball is fully contained in V .

We now complete the proof by showing that for any $x, z \in D, \epsilon > 0$ $A_{x,z}$ has probability one by showing that the complement

$$A_{x,z}^c := \{a \in A \mid |T^n(a, x) - z| > \epsilon \forall n \in \mathbb{N}\}$$

is a null set. With Lemma 7.3.7 we have for each image $y_x^j = T^j(a, x)$ at least one completing sequence $b(y_x^j, z)$ of length at most $M(\epsilon, \delta, \alpha, N)$ such that if $b(y_x^j, z)$ is a prefix of $\sigma^j(a) = a_{j+1}, a_{j+2}, \dots$ there exists a $n \leq j + M$ with $|T^n(a, x) - z| < \epsilon$.

In particular we have

$$\begin{aligned} A_{x,z}^c &\subseteq \{a \in A \mid b(y_x^j) \text{ is not prefix of } \sigma^j(a) \forall j \in \mathbb{N}\} \\ &\subseteq \{a \in A \mid b(y_x^{pM}) \text{ is not prefix of } \sigma^{pM}(a) \forall p \in \mathbb{N}\} =: C_{x,z}^\infty. \end{aligned}$$

Denote by $C_{x,z}^n$ the set

$$C_{x,z}^n = \{a \in A \mid b(y_x^{pM}, z) \text{ is not prefix of } \sigma^{pM}(a) \forall 0 \leq p < n\}.$$

Note that $C_{x,z}^{n+1} \subseteq C_{x,z}^n$ and $C_{x,z}^\infty = \bigcap_{n \in \mathbb{N}} C_{x,z}^n$. For the sets $C_{x,z}^n$ we can inductively

3 Generalized EHE model

derive upper bounds on their probability:

$$P(C_{x,z}^1) \leq 1 - \frac{1}{N^M} \text{ and } P(C_{x,z}^{n+1}) \leq P(C_{x,z}^n)(1 - \frac{1}{N^M})$$

It now follows by continuity from above that

$$P(A_{x,z}^c) \leq P(C_{x,z}^\infty) = \lim_{n \rightarrow \infty} C_{x,z}^n \leq (1 - \frac{1}{N^M})^n = 0$$

which completes the proof for a fixed ϵ . This is no problem however, since we can accommodate arbitrary small ϵ values using a countable intersection of the sets constructed here with respect to the ϵ levels $\epsilon_n = \frac{1}{n}$. \square

This almost sure topological transitivity paired with the uniform bernoulli shift is enough to ensure the ergodicity of the skew product dynamical system.

Theorem 3.6.3. *T is ergodic with respect to the product measure $\mu \times \lambda$, where μ is the uniform bernoulli measure on Σ_N and λ the uniform lebesgue measure on D. The same holds when using the one sided shift space Σ_N^+ .*

Proof. We have to show that for every two sets $E, H \subset \Sigma_N \times D$ of positive measure, there exists an $n > 0$ such that $(\mu \times \lambda)((T^{-n}E) \cap H) > 0$.

Let $m[i_0, \dots, i_n]$ denote a zylinder set on Σ_N following the notation in Einsiedler and Schmidt [2013].

$$m[i_0, \dots, i_n] := \{y = (y_m)_{m \in \mathbb{Z}} \in \Sigma_N \mid y_{k+m} = i_k \text{ for } k = 0, \dots, n\}$$

For every set E, H of positive $\mu \times \lambda$ measure we can find products of cylindersets on Σ_N and open sets on D contained in them. $m_e[i_0^e, \dots, i_{n_e}^e] \times U \subseteq E$, $m_h[i_0^h, \dots, i_{n_h}^h] \times V \subseteq H$.

For all $n > \max(m_e + n_e - m_h, 0)$ we have $\sigma^{-n}m_e[i_0^e, \dots, i_{n_e}^e] \subseteq m_h[i_0^h, \dots, i_{n_h}^h]$ and thus $\pi_{\Sigma_N}(T^{-n}(E)) \subseteq \pi_{\Sigma_N}(H)$.

Since T preserves the $\mu \times \lambda$ measure we have that $\mu \times \lambda(T^{-n}(E)) = \mu \times \lambda(\sigma^{-n}m_e[i_0^e, \dots, i_{n_e}^e] \times U') > 0$ and U' is a nonempty open set.

Thus we can apply Theorem 3.6.2 with U' and V and there exists an n_2 such that $\pi_D T^{n_2}(a, V) \cap U' \neq \emptyset$ and by continuity of $T(a_1, \cdot)$ for all $a_1 \in \mathcal{N}$ (with respect to the quotient topology) this intersection has positive measure for almost all $a \in \sigma^{-n}m_e[i_0^e, \dots, i_{n_e}^e]$.

Taken together we have $\mu \times \lambda(T^{-n-n_2}(E) \cap H) > 0$ proving the theorem. \square

3 Generalized EHE model

3.7 Probability Space for the avalanche patterns

In this section we will construct the probability space for the avalanches generated by the generalized EHE Model.

The sample space of the avalanches is given by Ω . Since Ω is a finite set we choose the powerset $\mathcal{F} = 2^\Omega$ as the sigma algebra.

In order to specify the probability measure it suffices to assign a probability to each elementary event $av \in \Omega$. Under the assumption of ergodicity, the probability of producing a specific avalanche av is proportional to the volume of the region $R(W, av)$ which can be directly calculated using (3.21):

$$\begin{aligned} \mathcal{V}(R(W, (G_i)_{i=1\dots D})) &= \Delta U \prod_{i=2}^D \prod_{j \in G_i} \left(\sum_{k \in G_{i-1}} w_{j,k} \right) \cdot \\ &\quad \left(\prod_{l \in \mathcal{N} \setminus \bigcup_{i=1}^D G_i} (1 - \sum_{l \in \bigcup_{i=1}^D G_i} w_{li}) - \right. \\ &\quad \left. \mathcal{V} \left(\Lambda \left(W, \mathcal{N} \setminus \bigcup_{i=1}^D G_i \right) \cap \left[0, 1 - \sum_{l \in \bigcup_{i=1}^D G_i} w_{li} \right]_{l \in \bigcup_{i=1}^D G_i} \right) \right). \end{aligned} \quad (3.28)$$

These volumes uniquely specify the probability space for all nonempty avalanches. The volume for the empty avalanche is given by

$$\sum_{i=1}^N \frac{1 - \Delta U - \mathcal{V}(\Lambda(W, \mathcal{N}) \cap [0, 1 - \delta[j=i]\Delta U]_{j \in \mathcal{N}})}{N}, \quad (3.29)$$

since external input to unit u_i doesn't start an avalanche in the region $[0, 1 - \Delta U)_i$ which has volume $1 - \Delta U$. This formula follows after subtracting the intersection of the non-inhabited volume with this region and averaging over all possible starting units i .

3.8 Avalanche size distribution for the homogeneous network

As an application of the framework derived in this chapter we see how the formula for the probability distributions reduce to the avalanche size distribution of the homogeneous EHE model Eurich et al. [2002].

3 Generalized EHE model

For the case of $W_{i,j}^{\text{hom}} = \frac{\alpha}{N}$, W has rank one and the formula for volume of the noninhabited region becomes very simple:

$$\mathcal{V}(\Lambda(W^{\text{hom}}, H) \cap [0, U_i]_{i \in H}) = \sum_{i=1}^{|H|} \frac{\alpha}{N} \prod_{j \in H, j \neq i} U_j$$

In particular we have for $\Lambda(W^{\text{hom}}, \mathcal{N})$

$$\mathcal{V}(\Lambda(W^{\text{hom}}, \mathcal{N})) = \alpha .$$

Formula (3.28) for the volume of the region $R(W^{\text{hom}}, \text{av})$ given an avalanche $\text{av} = (G_i)_{i=1,\dots,D}$ simplifies to

$$\mathcal{V}(R(W^{\text{hom}}, (G_i)_{i=1,\dots,D})) = \Delta U \underbrace{\prod_{i=2}^D \left(\frac{\alpha n_{i-1}}{N} \right)^{n_i}}_{I_1} \underbrace{\left(\left(1 - \frac{\alpha n}{N}\right)^{N-n} - \frac{N-n\alpha}{N} \left(1 - \frac{n\alpha}{N}\right)^{N-n-1} \right)}_{I_2(n)},$$

where $n_i = |G_i|$, $n = \text{size}(\text{av}) = \sum_{i=1}^D n_i$.

In order to find a closed form expression for

$$P(\text{size}(\text{av}) = n) \sim \sum_{\text{av} \in \Omega, \text{size}(\text{av})=n} \text{Vol}(R_{\text{av}})$$

note that only the factor I_1 in $\text{Vol}(R_{\text{av}})$ depends on the structure $(n_i)_{i=1,\dots,D}$ of av . Comparing with the recursion formula derived in Eurich et al. [2002] we get

$$\sum_{\text{av} \in \Omega, \text{size}(\text{av})=n} \prod_{i=2}^D n_{i-1} (\text{av})^{n_i(\text{av})} = \binom{N}{n} n^{n-1}$$

and

$$P(\text{size}(\text{av}) = n) \sim \Delta U I_2(n) \left(\frac{\alpha}{N} \right)^{n-1} \binom{N}{n} n^{n-1}$$

The possibility that the avalanche av occurs given that the current point in phase space is inside $R(W^{\text{hom}}, \text{av})$ is $1/N$ due to the uniform bernoulli measure of the external input. Taken together, this results in the (unnormalized) avalanche size distribution for size $n \geq 1$:

3 Generalized EHE model

$$\begin{aligned}
P(\text{size(av)} = n) &\sim \frac{1}{N} \binom{N}{n} n^{n-1} \Delta U \left(\frac{\alpha}{N} \right)^{n-1} \left(\left(1 - \frac{n\alpha}{N}\right)^{N-n} - \frac{N-n\alpha}{N} \left(1 - \frac{n\alpha}{N}\right)^{N-n-1} \right) \\
&= \frac{1}{N} \binom{N}{n} n^{n-1} \Delta U \left(\frac{\alpha}{N} \right)^{n-1} \left(1 - \frac{n\alpha}{N} \right)^{N-n-1} \left(1 - \frac{n\alpha}{N} - \frac{(N-n)\alpha}{N} \right) \\
&= \frac{1}{N} \binom{N}{n} n^{n-1} \Delta U \left(\frac{\alpha}{N} \right)^{n-1} \left(1 - \frac{n\alpha}{N} \right)^{N-n-1} (1 - \alpha).
\end{aligned}$$

In order to compute the normalization constant explicitly we compute the volume of the region not leading to an avalanche at all upon receiving external input and the total volume of inhabited phase space. For W^{hom} equation (3.29) simplifies to

$$P[\text{size(av)} = 0] \sim (1 - \Delta U) - \frac{N-1}{N} \alpha (1 - \Delta U) - \frac{\alpha}{N}.$$

Using this expression we can normalize the avalanche size distribution for size $n \geq 1$ to get

$$\begin{aligned}
P(\text{size(av)} = n) &= \frac{\frac{1}{N} \binom{N}{n} n^{n-1} \Delta U \left(\frac{\alpha}{N} \right)^{n-1} \left(1 - \frac{n\alpha}{N} \right)^{N-n-1} (1 - \alpha)}{(1 - \alpha) - (1 - \Delta U) + \frac{N-1}{N} \alpha (1 - \Delta U) + \frac{\alpha}{N}} \\
&= \frac{\frac{1}{N} \binom{N}{n} n^{n-1} \Delta U \left(\frac{\alpha}{N} \right)^{n-1} \left(1 - \frac{n\alpha}{N} \right)^{N-n-1} (1 - \alpha)}{(1 - \alpha) - (1 - \Delta U) + \alpha - \frac{N-1}{N} \alpha \Delta U} \\
&= \frac{\frac{1}{N} \binom{N}{n} n^{n-1} \Delta U \left(\frac{\alpha}{N} \right)^{n-1} \left(1 - \frac{n\alpha}{N} \right)^{N-n-1} (1 - \alpha)}{\Delta U \left(1 - \frac{N-1}{N} \alpha \right)} \\
&= \frac{1}{N} \binom{N}{n} \left(\frac{n\alpha}{N} \right)^{n-1} \left(1 - \frac{n\alpha}{N} \right)^{N-n-1} \frac{(1 - \alpha)}{\left(1 - \frac{N-1}{N} \alpha \right)},
\end{aligned}$$

which is equal to the formula [Eurich et al., 2002, Equation C21].

4 Summary and outlook

In this thesis we proposed a link between critical dynamics and feature integration in the brain. In particular this proposal considered networks in which subnetworks representing perceptual figures are embedded in such a way that upon activation by external input they display critical dynamics, whereas randomly chosen subnetworks or the system as a whole stay subcritical.

We were able to construct an algorithm that generates such a network using a generalization of the EHE model. We demonstrated that with multiple overlapping networks runaway activity quickly leads to a supercritical system showing 'epileptic' oscillatory states. This runaway activity could however be successfully contained when assigning negative weights to connections between units that do not share a common figure network and it was possible to embed a large number of figures. On average, a neuron could be connected to several figure networks. We analyzed the transition boundary to supercriticality and found that the probability of two units sharing a common subnetwork correlates very well with the phase transition.

In this thesis we only considered the problem of embedding multiple critical subnetworks of the same size. In this case we could use the known critical coupling strength from the homogeneous EHE model tuned to the figure size. However, extending this embedding scheme alone will be insufficient and strategies have to be devised if two figures with different sizes overlap. The framework derived in chapter 3 could in future be applied to this problem.

Afterwards we tested the separability of the dynamics of activated figure (target) networks from activated randomly chosen (background) networks in a simulated 2-alternative forced choice task. We found that the avalanche size distributions were clearly separate with critical distributions arising in the target stimulus. In addition, also the temporal dynamics were clearly separate between these two activation schemes even when the global firing rates in the two stimuli were made equal. A simple coincidence detector could distinguish with high accuracy between the target and distractor stimuli. These results were checked for robustness against higher level of background noise and lower levels of inhibition.

These results give a clear indication that critical subnetworks representing a figure offer good computational abilities for feature integration. Again we give as an outlook to go beyond the 2-AFC paradigm and to devise mechanism how not just the presence or absence of an activated figure network can be detected but also readout mechanism that can detect and recognize figure networks which become activated.

4 Summary and outlook

At the same time we deepened the mathematical understanding of the EHE model in this thesis, proving the ergodicity of the homogeneous network assumed in the derivations of the avalanche statistics from the volumes of phase space regions where they originate from [Eurich et al., 2002]. We were able to generalize this analysis for a large class of non-negative coupling matrices, in effect generalizing from one degree of freedom in the coupling matrix to N^2 . Still we could perfectly identify the non-inhabited region, prove that the system acts bijectively on its complement and identify the region leading to avalanches. We were able to derive a surprisingly structured formula for the volume of the non-inhabited region as an alternating sum of subdeterminants which could potentially lead to studies of the dependency of the network structure on criticality for networks with known spectral graph properties.

We also showed that there is a much simpler point of view to look at the generalized EHE model. We were able to completely transform away the internal spreading of activation by identifying the boundaries of regions leading to avalanches with the associated boundaries of their images.

It turned out that this identification leads to a quotient space homeomorphic to the N -torus. With respect to this topology the EHE model is just a shift in a random positive direction at each time step. In future, this connection to a random walk on the torus could be helpful to gain deeper insights into the generalized EHE system for example about the ergodicity in the non-homogeneous case.

Even if all regions leading to avalanches and their volume are known, it is a long way to go before one can use this to predict observed avalanche statistics in big networks. The number of possible avalanches in the system scales massively (quicker than the factorial function) so that closed form solutions for aggregate statistics of interest, for example avalanche size distributions have to be found for special cases. A particular simple case would be the derivation of the excitatory 2-ovl network, which would give theoretical insight into the expected crosstalk between overlapping subnetworks.

Bibliography

- Per Bak, Chao Tang, and Kurt Wiesenfeld.
Self-organized criticality: An explanation of the 1/f noise.
Physical review letters, 59(4):381, 1987.
- Claude Bedard, Helmut Kroeger, and Alain Destexhe.
Does the 1/f frequency scaling of brain signals reflect self-organized critical states?
Physical review letters, 97(11):118102, 2006.
- John M Beggs and Dietmar Plenz.
Neuronal avalanches in neocortical circuits.
Journal of neuroscience, 23(35):11167–11177, 2003.
- Nils Bertschinger and Thomas Natschläger.
Real-time computation at the edge of chaos in recurrent neural networks.
Neural Computation, 16(7):1413–1436, 2004.
doi: 10.1162/089976604323057443.
URL <https://doi.org/10.1162/089976604323057443>.
- Michael A. Buice and Jack D. Cowan.
Statistical mechanics of the neocortex.
Progress in Biophysics and Molecular Biology, 99(2):53 – 86, 2009.
ISSN 0079-6107.
- Thomas M Cover and Joy A Thomas.
Elements of information theory 2nd edition.
2006.
- Manfred Einsiedler and Klaus Schmidt.
Dynamische Systeme: ergodentheorie und topologische Dynamik.
Springer-Verlag, 2013.
- Christian W Eurich, J Michael Herrmann, and Udo A Ernst.
Finite-size effects of avalanche dynamics.
Physical review E, 66(6):066137, 2002.
- David J. Field, Anthony Hayes, and Robert F. Hess.
Contour integration by the human visual system: Evidence for a local “association field”.
Vision Research, 33(2):173 – 193, 1993.

Bibliography

ISSN 0042-6989.

Gerald Hahn, Adrian Ponce-Alvarez, Cyril Monier, Giacomo Benvenuti, Arvind Kumar, Frédéric Chavane, Gustavo Deco, and Yves Frégnac.
Spontaneous cortical activity is transiently poised close to criticality.
PLOS Computational Biology, 13(5):e1005543, 2017.

Leo P. Kadanoff, Sidney R. Nagel, Lei Wu, and Su-min Zhou.

Scaling and universality in avalanches.
Phys. Rev. A, 39:6524–6537, Jun 1989.
doi: 10.1103/PhysRevA.39.6524.
URL <https://link.aps.org/doi/10.1103/PhysRevA.39.6524>.

S Kauffman.

The origins of order: Self-organization and selection in evolution new york: Oxford univ, 1993.

Stuart A. Kauffman and Sonke Johnsen.

Coevolution to the edge of chaos: Coupled fitness landscapes, poised states, and coevolutionary avalanches.

Journal of Theoretical Biology, 149(4):467 – 505, 1991.

ISSN 0022-5193.

Chris G. Langton.

Computation at the edge of chaos: Phase transitions and emergent computation.

Physica D: Nonlinear Phenomena, 42(1):12 – 37, 1990.

ISSN 0167-2789.

Robert Legenstein and Wolfgang Maass.

Edge of chaos and prediction of computational performance for neural circuit models.

Neural Networks, 20(3):323 – 334, 2007.

ISSN 0893-6080.

Echo State Networks and Liquid State Machines.

Anna Levina.

A mathematical approach to self-organized criticality in neural networks.

PhD Diss, 2008.

Anna Levina, Udo Ernst, and J Michael Herrmann.

Criticality of avalanche dynamics in adaptive recurrent networks.

Neurocomputing, 70(10):1877–1881, 2007a.

Anna Levina, J Michael Herrmann, and Theo Geisel.

Dynamical synapses causing self-organized criticality in neural networks.

Nature physics, 3(12):857–860, 2007b.

Bibliography

- Wu Li and Charles D Gilbert.
Global contour saliency and local colinear interactions.
Journal of neurophysiology, 88(5):2846–2856, 2002.
- Norman H Packard.
Adaptation toward the edge of chaos.
Dynamic patterns in complex systems, 212:293–301, 1988.
- Thomas Petermann, Tara C Thiagarajan, Mikhail A Lebedev, Miguel AL Nicolelis, Dante R Chialvo, and Dietmar Plenz.
Spontaneous cortical activity in awake monkeys composed of neuronal avalanches.
Proceedings of the National Academy of Sciences, 106(37):15921–15926, 2009.
- Kaare Brandt Petersen et al.
The matrix cookbook.
- Viola Priesemann, Michael Wibral, Mario Valderrama, Robert Pröpper, Michel Le Van Quyen, Theo Geisel, Jochen Triesch, Danko Nikolić, and Matthias HJ Munk.
Spike avalanches in vivo suggest a driven, slightly subcritical brain state.
Frontiers in systems neuroscience, 8, 2014.
- Tiago L Ribeiro, Mauro Copelli, Fábio Caixeta, Hindiael Belchior, Dante R Chialvo, Miguel AL Nicolelis, and Sidarta Ribeiro.
Spike avalanches exhibit universal dynamics across the sleep-wake cycle.
PloS one, 5(11):e14129, 2010.
- D.L. Schacter, D. T. Gilbert, and D. M. Wegner.
Psychology (2nd Edition).
Worth, New York, 2011.
- Woodrow L Shew and Dietmar Plenz.
The functional benefits of criticality in the cortex.
The neuroscientist, 19(1):88–100, 2013.
- Nergis Tomen, David Rotermund, and Udo Ernst.
Marginally subcritical dynamics explain enhanced stimulus discriminability under attention.
Frontiers in systems neuroscience, 8, 2014.
- Jonathan Touboul and Alain Destexhe.
Can power-law scaling and neuronal avalanches arise from stochastic dynamics?
PLOS ONE, 5(2):1–14, 02 2010.
- Rufin VanRullen, Arnaud Delorme, and Simon Thorpe.
Feed-forward contour integration in primary visual cortex based on asynchronous spike propagation.
Neurocomputing, 38:1003–1009, 2001.

Bibliography

Johan Wagemans, James H Elder, Michael Kubovy, Stephen E Palmer, Mary A Peterson, Manish Singh, and Rüdiger von der Heydt.

A century of gestalt psychology in visual perception: I. perceptual grouping and figure-ground organization.

Psychological bulletin, 138(6):1172, 2012.

Max Wertheimer.

Untersuchungen zur Lehre von der Gestalt. II.

Psychologische forschung, 4(1):301–350, 1923.

Shih-Cheng Yen and Leif H Finkel.

Extraction of perceptually salient contours by striate cortical networks.

Vision research, 38(5):719–741, 1998.